Instituto Superior Técnico

Licenciatura em Engenharia Física Tecnológica

Application of Magnetic Reading Technology in New Biochip Development

---

Hugo Ferreira

Lisboa, July 2001

Abstract

Spin-valve sensors, traditionally used in Magnetic Recording/Reading Technology for disk and tape drives were used in the development of a new biochip. This novel approach makes use of the Giant Magneto-Resistive (GMR) effect of the sensor for detecting nano- and micrometer sized superparamagnetic particles with biomolecules immobilized on their surface. The controlled movement and specific placement of the particles and their detection was successfully demonstrated. More significantly, the sensors used were sensitive enough to detect single particles, envisioning future applications in DNA screening, drug target studies, protein analysis and more.

Resumo

Os sensores válvula-de-spin usados tradicionalmente na Tecnologia de Gravação/Leitura Magnética nas “drives” para disco rígido ou fita magnética foram usados no desenvolvimento de um novo biochip. Esta nova aplicação usa o efeito Magneto-Resistivo Gigante (MRG) dos sensores na detecção de partículas super-paramagnéticas de tamanhos nano e micrométricos que possuem biomoléculas imobilizadas na sua superfície. O movimento e posicionamento das partículas em áreas adjacentes aos sensores foram controlados e a sua detecção foi demonstrada com sucesso. Em especial, a detecção de partículas isoladas foi conseguida, perspectivando-se novas aplicações no “screening” de DNA, pesquisa de novas drogas, análise de proteínas entre outras.

Publications

This work has given rise so far to two accepted papers in Journal of Applied Physics to be published in 2002.

- D.L. Graham, H.A. Ferreira, J. Bernardo, P.P. Freitas, J.M.S. Cabral, "Single magnetic microsphere placement and detection on-chip using current line designs with integrated spin valve sensors: biotechnological applications", submitted to Journal of Applied Physics, September 2001.
- L. Lagae, R. Wirix-Speetjens, J. Das, H.A. Ferreira, D.L. Graham, P.P. Freitas, G. Borghs, J. De Boeck, "On-chip manipulation and magnetization assessment of magnetic bead ensembles by integrated spin-valve sensors", submitted to Journal of Applied Physics, September 2001.

The first of these papers follows directly from the presented work. The second one results from the continuation of an internship's work performed by this reports' author with Roel Wirix-Speetjens, a belgian student that spent the Summer of 2000 at INESC.

Furthermore, the works on these papers are going to be presented in the 46^{th} Annual Conference on Magnetism and Magnetic Materials next November: the first one as an oral presentation by this report's author and the second one as a poster.

Acknowledgements

Firstly, I would like to thank Professor Paulo Freitas for providing a role for me in this project and for his useful supervision. This work has provided me with the opportunity to gain confidence in my ability to do challenging scientific research.

Secondly I want to thank Dr. Daniel Graham for is support and companionship throughout this work, and most of all for making it more enjoyable.

I also want to thank the technicians of the Centre for Microsystems and Nanotechnologies (Centro de Microsistemas e Nanotecnologias) the former Solid State Technology Group (Grupo de Tecnologia de Estado Sólido) for helping me with chip processing, namely Fernando Silva, José Bernardo and Virgínia Soares.

I would also like to thank Sr. José Faustino for chip mounting, wire bounding and his help with the experimental setup.

My thanks also go to my collegues in the Center for Microsystems and Nanotechnologies for their occasional help and advice, namely Anabela Veloso, Haohua Li, Jianguo Wang, Ricardo Sousa, Zhengang Zhang, Zongzhi Zhang and Susana Cardoso, whom I thank also for wafer dicing.

I am also grateful to the Instituto de Engenharia de Sistemas e Computadores (INESC) for providing the facilities for the realization of this work and likewise the Centro de Engenharia Biológica e Química for the use of their biochemistry laboratories.

This work was partly funded by the project POCTI/34459/BIO/2000 – "Detection of Biomolecular Recognition in Nanometer Sized Volumes using Magnetoresistive Sensor Arrays", to which I am very thankful.

A great acknowledgement to my parents, Mª Regina e Jorge Ferreira, and to my brother, Ricardo, for their presence in my life and for supporting me in the pursuit of my childhood's dream of becoming a scientist. I hope I made you proud of me!

Finally, a special thanks to my wife, Catarina Escobar, who has been an irreplaceable inspiration throughout my course and through this work. I hope that a happy future waits for us together!

Motivation

The work outlined in this report represents the final year project study of my Licenciatura em Engenharia Física Tecnológica (Engineering Physics Course). This project is the continuation of work performed during the course of Microtecnologias (Microtechnologies): “Partículas Nano-Magnéticas” (“Nano-magnetic Particles”).

Both projects were supervised by Prof. Paulo Freitas, who received me in his research group, Centre for Microsystems and Nanotechnology (former Solid State Technology Group), which is part of INESC – Instituto de Engenharia de Sistemas e Computadores (Institute for Systems and Computers Engineering)

This project encompasses two of my favourite areas of science: Physics and Biology. When I applied for the physics course 6 years ago I applied secondly for Biochemistry with the intention of pursuing the study of genetics. Fortunately, life has given me the chance to do something in between these two areas! Furthermore, these whole 5 years in the Physics course has awakened in me the liking for things in small scale leading me to dream about Nanotechnology. This project represents something that appealed to my “needs” and I hope to remain involved in nano-biotechnology for years to come. To this end I have recently been awarded a Ph.D. grant to continue this work at INESC. Lets see what the future holds.

O Sonho de Pigmaleão

Surgiste-me bela e misteriosa,
difusa como a luz de um dia enevoado.
Olhei-te de alto a baixo,
sustendo a respiração ...
prestando atenção a todos os pormenores ...
Vi que os outros também te procuravam,
pareciam perceber-te ...
e contigo trocavam palavras de amor.
Suspirei ...
Também eu queria admirar-te.
Moldar-te com os meus lábios.
Suavizar o traço dos teus olhos.
Colorir as maçãs do teu rosto.
Entender o teu sorriso.
Fazer-te também minha.
Tornar-te mais bela,
e depois ...

Fazes-me sonhar,
O Sonho de Pigmaleão.

Contents

Abstract / Resumo 2
Publications 3
Acknowledgments 4
Motivation 5
1. Introduction 8
2. Physical Background 10
2.1 Spin-valve sensor 10
2.1.1 Principles 10
2.1.2 Characterization 12
2.2 Current lines 14
2.3 Superparamagnetic particles 15
2.3.1 Magnetic moments 17
3. Biochemical Background 18
3.1 Biomolecule tagging 18
3.1.1 Enzyme activity 20
3.2 Surface immobilization 21
4. The Circuit 25
4.1 Design 25
4.2 Processing 27
4.3 Mounting 32
5. The Experiments 34
5.1 Experimental setup 34
5.2 Bead alignment in magnetic field 35
5.3 Controlled movement 36
5.4 Detection 37
5.4.1 Expected signal 37
5.4.2 Experimental detection 40
5.4.3 Detection of biomolecular recognition 42
6. Conclusions and Future Perspectives 45
Bibliography 48
Appendix 50
A. Immobilization Procedures 51
B. Run-sheets 54
C. Process schematics 66

1. Introduction

Nowadays, one is presented with a fast and faster miniaturization of all sorts of devices. These small devices are already so present in one's daily life that their existence is often forgotten: they've become a constant and invisible companion to the human species (at least in the 1st world countries). But the future will make this "bond" even stronger with the development of tiny machines and devices that are present in one's clothes or even inside our blood vessels repairing tumours, in an almost "symbiotic" kind of liaison.

One familiar example of these small devices is the hard disk drive. This device is a complex instrument, which includes a slider with the recording/reading head (Fig. 1.1) ([1]), which writes and reads data to and from the hard disk media (Fig 1.2). The reading head is composed of magnetic nanostructures, one of which is the spin-valve sensor, responsible for the reading of the magnetic field generated from the bits in the hard disk media ([2], [3], [4], [5]).

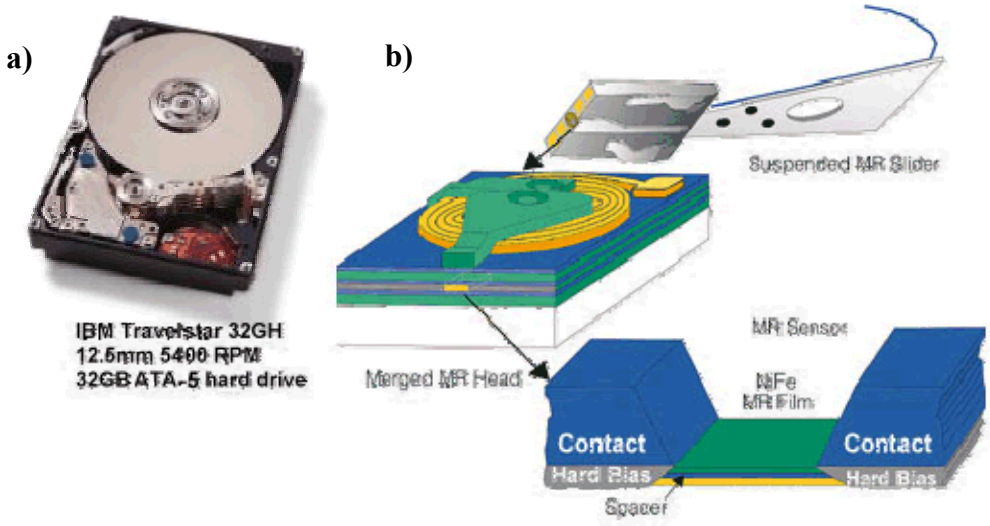

Fig. 1.1: a) A hard disk drive. b) Hard disk slider showing the reading MR head in detail.

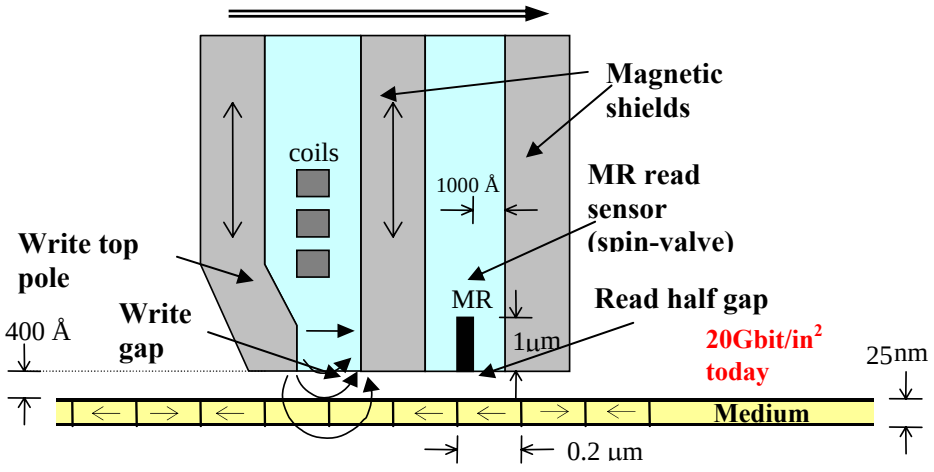

Fig. 1.2: Hard disk's recording/reading head scheme, showing the MR element.

The main objective of the presented work is to use this kind of sensor in a new application apart from the traditional domain of magnetic recording/reading technology: the development of a new type of biochip! The spin-valve sensors are to be used in the detection of the magnetic field generated by superparamagnetic particles with biomolecules immobilized in its surface. A further objective of this work is to control the movement and positioning of these particles.

The approach of using this kind of sensors in biochips has already been proposed ([6], [7], [8], [9]), but this work represents the first real use of these sensors for the detection of magnetic particles, with or without biomolecules immobilized.

This report includes brief introduction, physical and biochemical background information, circuit and biochip fabrication details, results on the controlled movement and sensing of magnetic particles and the relevant conclusions and future perspectives of the work.

2. Physical Background

In this chapter some physical aspects of this work will be considered, such as the structure and function of the spin-valve sensor, the current line features and the nature of the superparamagnetic particles used in this work.

2.1 Spin-valve sensor

The spin-valve sensors were first introduced in 1991 ([10]) and they were first developed and tested in 1994 ([11]). Since then, they have been used in several applications, mainly in read heads for hard disk and tape, but also in devices for controlling the rotational velocity of ABS systems or controlling the position of robotic systems and in the monitoring of high tension cables ([12]). Now, they are starting to be used in the study of biological systems – biosensors and biochips!

2.1.1 Principles

In 1986 it was observed ([13]) that two magnetic layers separated by a nonmagnetic spacer layer could display a spontaneous antiparallel alignment of the magnetizations at zero field, the so called antiferromagnetic interlayer exchange coupling. Directly after this discovery it was shown ([14]) that a large change in resistance could occur when the antiparallel alignment is changed to parallel (and vice-versa) with an externally applied field. This change in resistance is much larger than can be expected for "normal" magnetoresistance, caused by Lorentz forces, or for the anisotropic magnetoresistance effect, caused by spin-orbit interactions. Therefore, this effect became known as Giant MagnetoResistance (GMR).

The origin of the GMR effect lies in the spin-dependent transmission of conduction electrons between the coupled magnetic layers through the nonmagnetic spacer, which depends on the relative orientation of the moments of the magnetic layers, as can be seen in Fig. 2.1 ([15]) for two magnetic layers separated by a nonmagnetic layer.

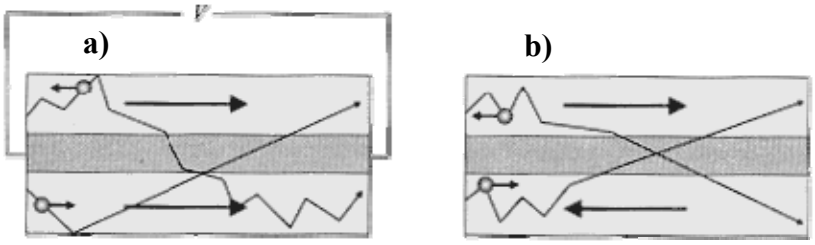

Fig. 2.1: Schematic drawing of the current-in-plane GMR effect in two magnetic layers separated by a nonmagnetic spacer layer with a) parallel and b) antiparallel magnetizations. The electrical transport in the layers can be divided in two spin-channels, illustrated as two electrons with different spin direction moving from the left to the right in the layers. Electrons with their spin opposite to the local magnetization direction experience more resistance than electrons with their spin parallel to the magnetization. In case of parallel magnetizations one current channel acts a shunting current.

This trilayer structure is often referred to as a spin-valve. The electrical transport in the layers can be divided in two spin-channels, currents resulting from spin-up and spin-down electrons. These two types of electrons have two different

scattering probabilities at the interfaces and in the bulk of the layers, due to a spin-dependent potential landscape and differences in the density of states at the Fermi-level. In general, an electron will have a higher scattering probability when its spin direction is opposite to the local magnetization direction. When both magnetic layers have parallel moments, in Fig. 2.1a, the spin-down electrons will have a higher scattering probability then the spin-up electrons. This spin-up channel acts as a shunting current, which lowers the resistivity of the complete stack of layers considerably as compared to the situation when the moments are antiparallel, as in Fig. 2.1b. In this latter case both spin-up and spin-down electrons will have a high scattering probability in one magnetic layer and a low scattering probability in the other. The relative change in resistance, the GMR-ratio, or simply MR-ratio, is usually defined as

$$MR = \frac{R_{AP} - R_P}{R_P} \tag{2.1}$$

with R_{AP} and R_P the resistance of the stack of layers with antiparallel (AP) and parallel (P) state of magnetizations, respectively. As illustrated by Fig. 2.2 ([16]), one can see a maximum relative change in resistance when the alignment of the magnetic layers is antiparallel and a minimum relative change when the alignment is parallel. The MR signal of the spin valve sensors used in this work was approximately 5%.

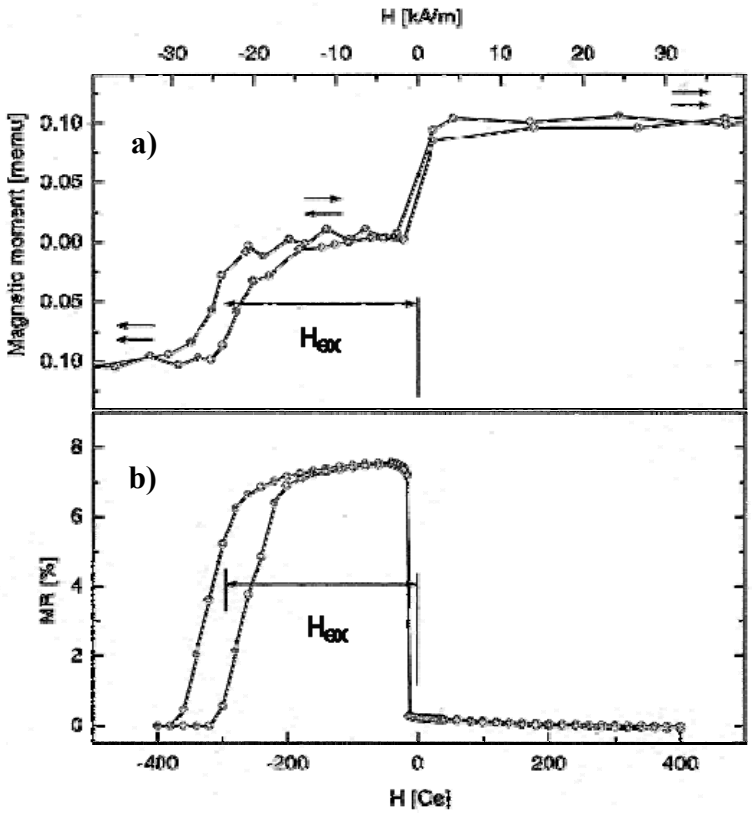

Fig. 2.2: Plots of the magnetic moment a) and relative change in resistance b) of a spin-valve structure in function of the applied field. The application of the external magnetic field changes the relative orientation of the magnetic layers magnetizations. One can see that when the magnetization directions of the magnetic layers are antiparallel the MR change is maximum and when there are parallel the MR signal is minimum.

2.1.2 Characterization

The spin-valve sensors have the structure Ta20Å/NiFe30Å/CoFe20Å/Cu28Å/ CoFe25Å/MnIr60Å/Ta25Å, as can be seen in Fig. 2.3.

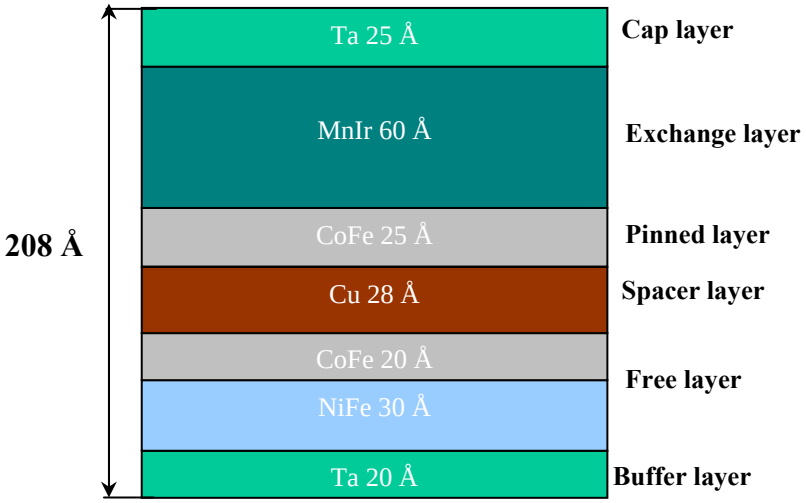

Fig. 2.3: Top spin-valve structure used in the presented work

The bottom Ta layer in the structure is used as a buffer to induce the right crystalline growth of the subsequent layers. The NiFe and CoFe layers behave as one magnetic layer in the sensor, which is called the "free" layer. The Cu layer is the nonmagnetic spacer of the spin-valve structure discussed above. The top CoFe layer is the second magnetic layer coupled to the free layer below and is called the "pinned" layer. The MnIr ([17]) is an antiferromagnetic layer that couples, via an exchange field, the pinned layer. Finally, the top Ta layer acts as a protective layer on the top surface of the sensor structure

The effect of coupling of the MnIr layer to the CoFe layer is that it pins the magnetization direction of the CoFe layer. In this way, the alignment of the magnetization doesn't change with an external applied field unless the field value is larger than the exchange field (as seen in Fig. 2.2), thus the name pinned layer. Since the NiFe/CoFe layer is not coupled by exchange to the MnIr layer, it is free to rotate under a magnetic applied field, thus the name free layer. As the pinned layer is on top of the free layer this structure is called top spin-valve.

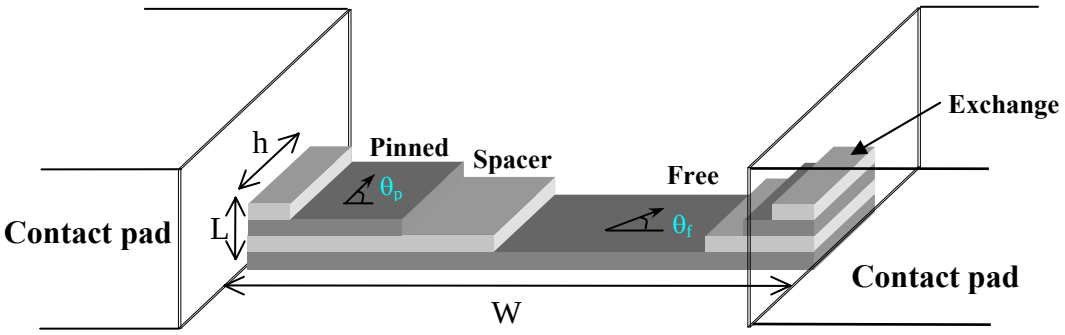

Fig. 2.4: Schematic of a spin-valve sensor, focusing the Exchange, Pinned, Spacer and Free layers, and where *W*, *L* and *h* are the width, the length and the height of the sensor, respectively. θ_f and θ_p are the angles that the magnetization of the free and pinned layers, respectively, do with the direction of the sense current (along the width of the sensor).

In defining a spin-valve sensor a bulk sample of the spin-valve material is patterned to obtain the required geometry. Fig. 2.4 shows a scheme for a spin-valve sensor, with the alignment of the magnetic layers exposed and where *W*, *L* and *h* are the width, the length and the height of the sensor, respectively.

A typical sensor transfer-curve, obtained in this work, is presented in Fig. 2.5.

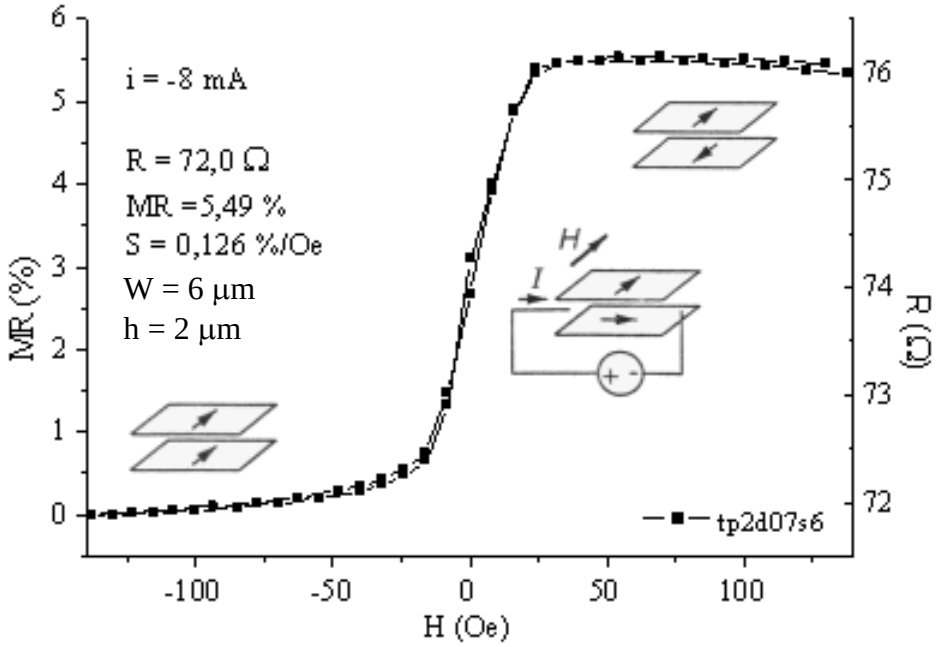

Fig. 2.5: Typical sensor transfer-curve obtained in the presented work. The sensor has a minimum resistance of 72.0Ω, an MR signal of 5.49% and a sensitivity *S*~0.13%. Inset: the sensor was biased with a sensor current *I* of 8mA, so the magnetization directions of the magnetic layers are perpendicular at zero applied field; also, the MR signal is maximum/minimum for antiparallel/parallel alignment of the magnetic layers.

The resistance of the sensor is given by

$$R_{SV} = R_{sqr}\frac{W}{h}\left(1-\frac{MR}{2}\right)\left\langle\cos\left(\theta_f-\theta_p\right)\right\rangle \qquad (2.2)$$

where R_{SV} is the electrical resistance of the spin-valve sensor; R_{sqr} is the sheet resistance of the spin-valve film, defined as ρ_0/L, with ρ_0 the resistivity of the film and L the length of the sensor, which is also the total thickness of the film; θ_f and θ_p are the respective angles for the magnetization of the free and pinned layers, with the direction of the current I (along the width of the sensor); and < > represents the average of $\cos(\theta_f - \theta_p)$ along the height h of the sensor, since the demagnetizing fields are not uniform along that dimension, and so are the referred angles. The output of the sensor, in voltage, will then be

$$\Delta V = R_{sqr} I\frac{W}{h}\frac{MR}{2}\left\langle\cos\left(\theta_f-\theta_p\right)\right\rangle \qquad (2.3)$$

Usually, without an external applied field, the magnetization of the pinned layer is almost perpendicular to width of the sensor ($<\theta_p>$~90º) and the magnetization of the free layer is close to the direction of the current ($<\theta_f>$~0º), for a biased sensor. This biasing is accomplished by applying a current to the sensor (see Fig. 2.5). It is also shown that sensors with a big ratio W/h (W/h<4 and h>3μm) have demagnetizing fields large enough to stabilize the alignment of the free layer along the width of the sensor.

In order to measure the small magnetic fields generated by the superparamagnetic particles, we defined the working area of the sensor as the linear region where the change in resistance of the sensor is proportional to the applied field. This region was centred around zero applied field i.e. the sensor was biased. The biasing current was found to be 8-10mA in the experiments performed. Thus, with $<\theta_p>$~90º and for the biased sensor, $<\theta_f>$~0º, at zero applied field, the sensor only detects magnetic fields in the direction along the height of the sensor. Only fields in this direction will be able to rotate the free layer to the direction of the pinned layer, in the linear range. Under these conditions the sensor response will vary simply with a function of :

$$R_{SV} = R_{sqr}\frac{W}{h}\left(1-\frac{MR}{2}\right)\left\langle \sin\theta_f \right\rangle \tag{2.4}$$

$$\Delta V = R_{sqr} I \frac{W}{h}\frac{MR}{2}\left\langle \sin\theta_f \right\rangle \tag{2.5}$$

For the pre-biased sensor the value of $\sin\theta_f$ is related to the external applied field in the following manner:

$$\left\langle \sin\theta_f \right\rangle = \begin{cases} \dfrac{H_{ext}}{H_D^f - H_k} & , if\ \ H_D^f > H_k \\ \pm 1 & , if\ \ H_D^f \le H_k \end{cases} \tag{2.6}$$

where H_{ext} is the external applied field, H^f_D, is the shape demagnetization field and H_k is the anisotropy field. The values ± 1 for $\sin\theta_f$ indicate that the sensor is saturated; this is, not in the linear region.

One can now define the sensitivity S of the spin-valve sensor as the slope of the linear region of the sensor's response. The sensitivity will then be expressed as %/Oe (% resistance change), as can be seen in Fig. 2.5.

2.2 Current lines

It is already known that when a metal is subjected to an electrical current a magnetic field is generated, as translated by Fig. 2.6 and Eq. 2.7 (S.I. units) ([18]).

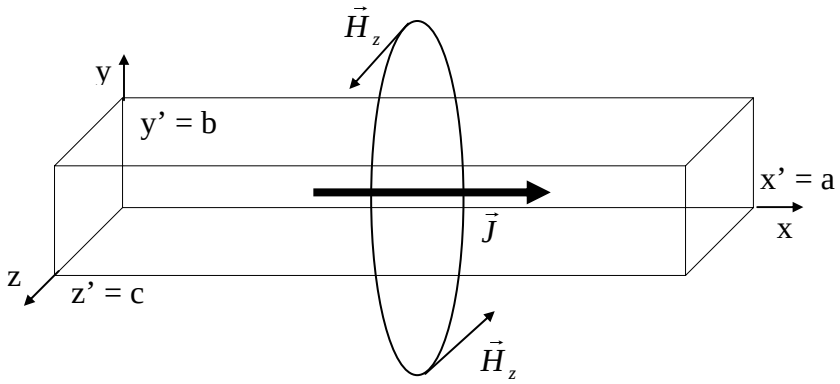

Fig. 2.6: Schematic of a metal bar current line and the field generated by the density of current $\vec{J}$.

$$\vec{H}(\vec{r}) = \frac{1}{4\pi}\int_{V'}\frac{\vec{J}(\vec{r}')\times\hat{R}}{R^2}d\vec{r}' \qquad (2.7)$$
$$\vec{R} = \vec{r} - \vec{r}'$$

Consequently, in order to control the movement and positioning of the superparamagnetic particles, we used Al current lines integrated on the chip. It will be seen further on that a particular geometry for the current lines was used to fulfil the requirement.

2.3 Superparamagnetic particles

The particles and beads used in this work are superparamagnetic. This means that when no external field is applied to the particles they have zero magnetic moment, but in the presence of a non-zero applied field the beads will have a non-zero moment. This happens because the particles are made from a polymer matrix with iron oxide (magnetic) grains within. These are not coupled ferromagnetically, conferring the particles the paramagnetic behaviour. Without the presence of an applied field the magnetic grains' moments are randomly distributed so the resulting magnetic moment is null, with an applied field all the grains' moments become aligned with the field so that the resulting moment is different from zero, as illustrated in Fig. 2.7:

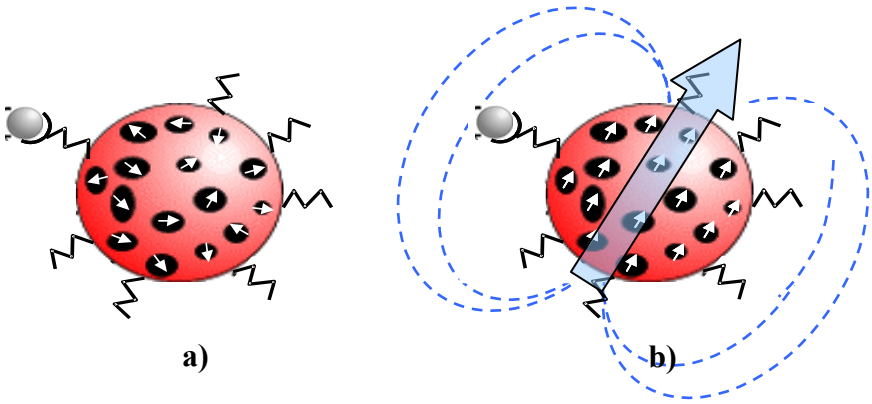

Fig. 2.7: Schematic of the magnetic particles used in this work. The beads are made from a polymer matrix with magnetic grains within. Without an external magnetic field applied the grains' magnetic moments are randomly distributed resulting in a null particle's moment a), while in the presence of a field the grains align in the direction of the field resulting in a non-null moment b).

Two kinds of magnetic particles were used: 400nm dextran-iron oxide (70%) particles (Nanomag®-D, Micromod) and 2μm polymer encapsulated iron oxide (15%) microspheres (Micromer®-M, Micromod) ([19]). The distinction between particles and microspheres is made due to the irregular shape of the former and the regular, spherical shape of the latter. The suppliers' characteristics of these particles and microspheres are presented in the table below (Table 2.1):

400nm particles (Nanomag®-D)	**2μm microspheres (Micromer®-M)**
Bell-shaped size distribution: 200-600nm	very uniform size and shape: spherical
70-80% magnetite + maghemite cross-linked with dextran	micro-coned magnetite 15% in co-polymer composite
stock : 83 mg/ml particles	stock : 25mg/ml microspheres
density : 4.0g/ccm	density : 1.4g/ccm
saturation magnetization : >60emu/g (H>10,000 Oe)	saturation magnetization : >34emu/g (H>10,000 Oe)

Table 2.1: Characteristics of the beads used in the work supplying by the company of origin.

and their behaviour under an external magnetic field is shown in Fig. 2.8:

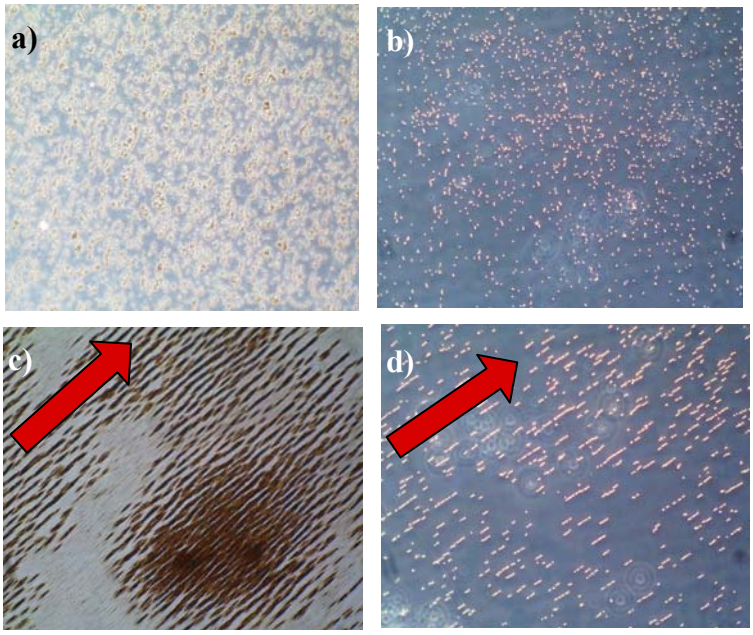

Fig. 2.8: Behaviour of particles in the absence or in the presence of an external field (arrow) for 400nm particles, a) and c), and for 2μm particles, b) and d).

It is immediately apparent, even with zero applied external field, that the 400nm particles have a tendency to aggregate. This disadvantageous feature, as will be explained, favours the use of the 2μm particles in some of the experiments performed.

2.3.1 Magnetic moments

Saturation magnetization data for both types of particle was provided by the supplier (Micromod), but additional experiments were performed to confirm the magnetization at low fields and ultimately to determine the magnetic moment per particle.

The magnetic moment of both types of beads was determined by drying 40μl liquid samples of known stock particle suspensions (25 or 83mg/ml) in a vacuum oven at 100ºC for 1 hour, measuring the dry weight of the samples and then performing a magnetic susceptibility measurement with a VSM in the ±100Oe range. Examples of the plots obtained with VSM are shown in Fig. 2.9a and b for both types of particles.

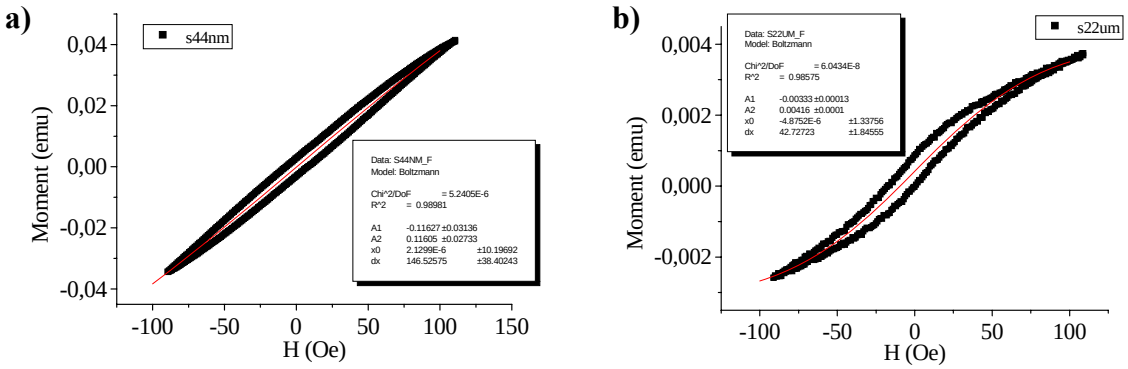

Fig. 2.9: VSM measurements of bulk dried samples of a) 400nm particles and b) 2μm microspheres.

The moment of the samples at a specified field was measured directly from the plots and also by fitting a sigmoidal (boltzmann) curve to the plots, obtaining similar results for both approaches: ~0.9emu/g for the 2μm microspheres and ~3.7emu/g for the 400nm particles for an applied field of ~15Oe. This field value was equivalent to that used in the detection experiments, as discussed in section 5.2.

The moment per particle or bead was calculated using the supplier's data on the density and number of particles per unit weight (it was assumed that both types of particles were spherical in shape): $\sim 5\times10^{-12}$emu/2μm bead and $\sim 5\times10^{-13}$ emu/400nm particle. It was noted that, although the 2μm microspheres have a higher moment per particle than the 400nm beads, they have a smaller moment per weight, which is easily explained by the higher density of the latter particles.

Finally, for small values of the applied field, the determined magnetic susceptibility was $\chi\sim0.06$emu/(g·Oe) for the 2μm particles and $\chi\sim0.25$emu/(g·Oe) for the 400nm particles.

3. Biochemical Background

The magnetic particles and microspheres were employed as both carriers and labels for the biomolecules of interest. As carriers the particles provided a means of transporting the attached biomolecules to specific sites on the chip and as labels the particles allowed the detection of the presence of the biomolcules at sensor sites. For the purposes of biomolecule attachment (termed “immobilization” in biochemistry) a variety of particle surface functionalizations are possible, enabling the immobilization of different biomolecules via different chemical procedures. This chapter will focus on the biochemistry issues related to this work: The immobilization of biomolecules to magnetic particles or substrate surfaces, the subsequent determination of biomolecule (enzyme) activity and the binding of magnetic particles to substrate surfaces via biomolecular interaction (streptavidin-biotin).

3.1 Biomolecule tagging

Magnetic beads, such as the ones used in this work, have been largely used in biomolecular separation processes through their biochemical surface functionalization ([20]), however the detection of magnetically labelled biomolecules is new (see Fig. 3.1 for uses giving to the studied particles).

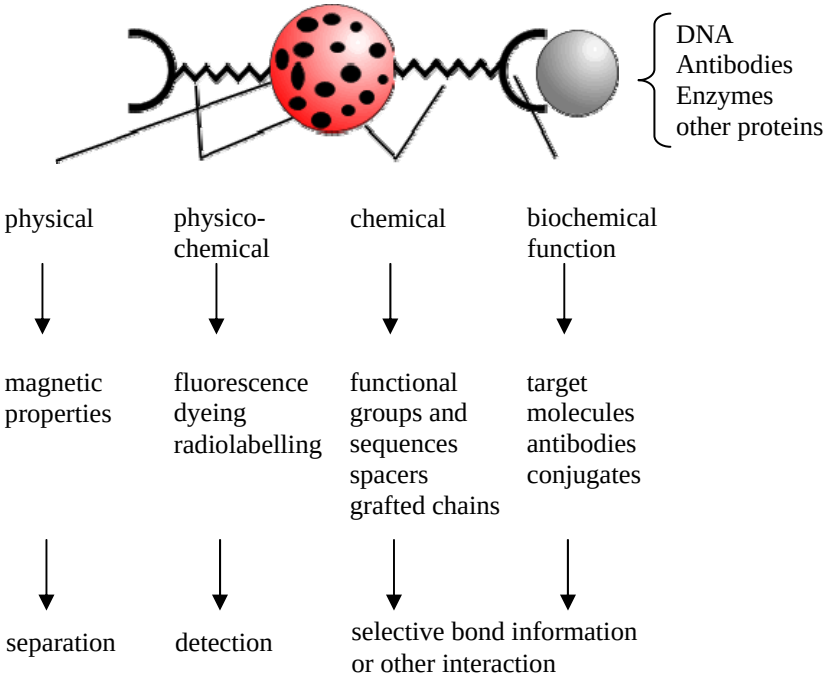

Fig. 3.1: Traditional uses and applications given to the magnetic particles

Surface functionalization and subsequent immobilization allows the magnetic labelling of a large number of biomolecules, like DNA, RNA, antibodies, enzymes and other proteins.

As a starting point a model biomolecule was used to illustrate the magnetic labelling and its detection: This was the analytical enzyme Horseradish Peroxidase (HRP, classification number E.C.1.11.1.7.) ([21]). The reasons for this choice include the low price and high purity of the enzyme and the fact that it has been well studied

(see Table 3.1 for its properties and Fig. 3.2 for a schematic of the enzyme bound to the beads surface).

Horseradish Peroxidase (HRP) **E.C.1.11.1.7**
Cheap and commercially available Small (medium weight 44kDa ; Stokes radius 27Å) Amino acid sequence known Assay methods readily available Can be stabilized in aqueous or organic solvents

Table 3.1: Properties of the model biomolecule: the Horseradish Peroxidase (HRP) enzyme.

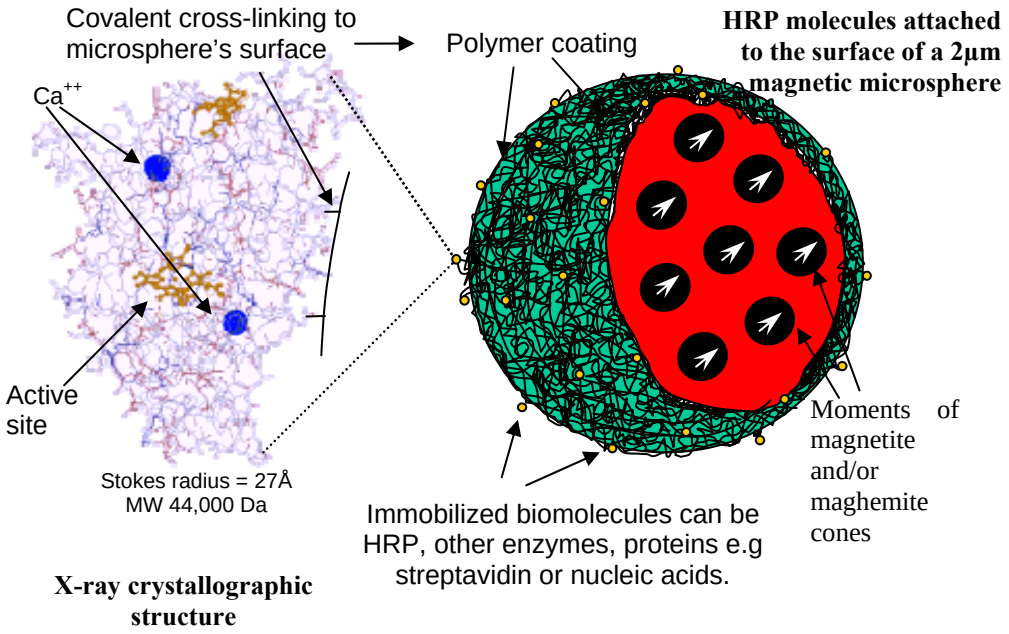

Fig. 3.2: Schematic showing the immobilization of HRP molecules to a 2µm microsphere. An enlargement of the immobilization shows the X-ray crystallographic structure of the enzyme.

The immobilization of HRP to superparamagnetic particles can be performed using several procedures. Two approaches were employed here, each based on the functional groups on the surface of the particular particles. HRP was bound to Nanomag®-D particles functionalized with free carboxyl groups using the negatively charged polymer polyethylenimine, the cross-linking reagent glutaraldehyde and para-benzoquinone. HRP was also immobilized to Micromer®-M microspheres with free amino functionality using the common glutaraldehyde methodology (see Fig. 3.3).

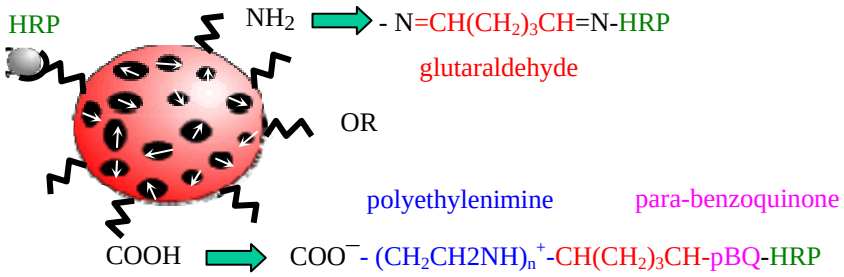

Fig. 3.3: Two methodologies for immobilization of HRP molecules in the 2μm beads: either the particles' surface has amino or carboxylic groups.

3.1.1 Enzyme activity

One question that might arise from the immobilization of HRP to the magnetic labels is whether or not the enzyme remains active. That is, the enzyme may bind in an active or inactive way, according to whether the active centre of the enzyme remains functional or not (this structural region, termed the "active site", is responsible for the catalytic activity of the protein). Inactivity may result from a conformational change in the protein structure or more simply by the active site being blocked in some way e.g. by proximity to the particle surface or by interacting with the polymer content of the particle. This blocking is termed "steric hindrance".

To determine the activity of immobilized HRP an adapted form of the guaiacol assay was used. This is a spectrophotometric method based on the production of a coloured product, which can be measured by its absorbance at a particular wavelength of light. HRP in the presence of hydrogen peroxide degrades a substance known as Guaiacol (2-methoxyphenol) into an amber coloured product which absorbs strongly in the 400-500nm region of the spectrum. The reaction can be written as follows:

$$\text{(free) HRP} + H_2O_2 + \text{Guaiacol} \rightarrow \text{"amber colored" product} \qquad (3.1)$$

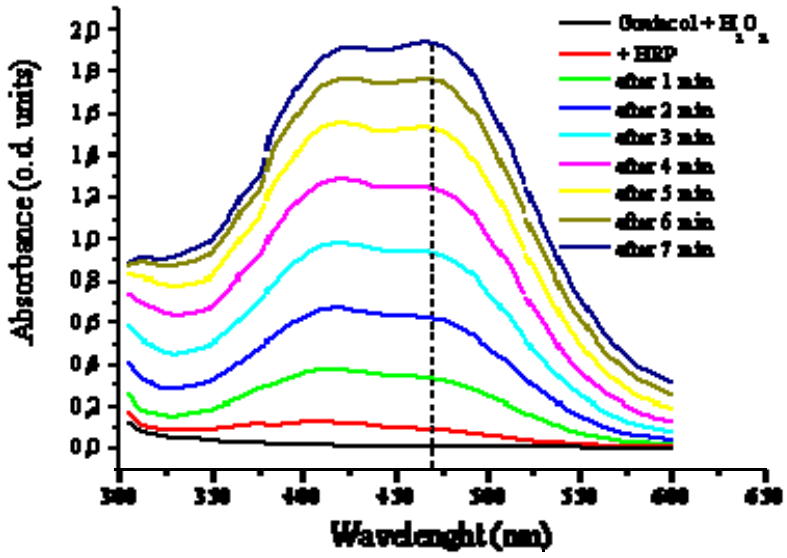

Fig. 3.4: UV/VIS measurements for the HRP degradation of guaiacol in function of time. In black, the absorption vs wavelength for a solution with just Guaiacol and hydrogen peroxide; the addition of HRP to the solution (red curve); remaining curves absorption for different times after HRP addition.

Fig. 3.4 shows a series of UV/visible scans of the reaction solution with a function of time. The amber colored product has two absorption peaks around 420 and 470nm. Hence, the guaiacol assay is based on the rate of change of absorbance at 470nm. The rate determination reactions are carried out in 2ml of phosphate buffer (100mM, pH7, rt) containing 2.5mg/ml guaiacol placed in 3ml quartz cuvettes. The enzyme sample is added e.g. 20µl of a known concentration (0.1, 0.02 or 0.01mg/ml) of HRP or 20µl of HRP-particle suspension, the absorbance is zeroed and the reaction initiated via the addition of 2µl of hydrogen peroxide (3% solution). The reactions are performed in a spectrophotometer at room temperature. Both HRP immobilized to particles and microspheres were assayed this way. Fig. 3.5 shows the plots obtained for these measurements, with Fig. 3.5b showing a close-up of Fig. 3.5a for the lower absorbance changes.

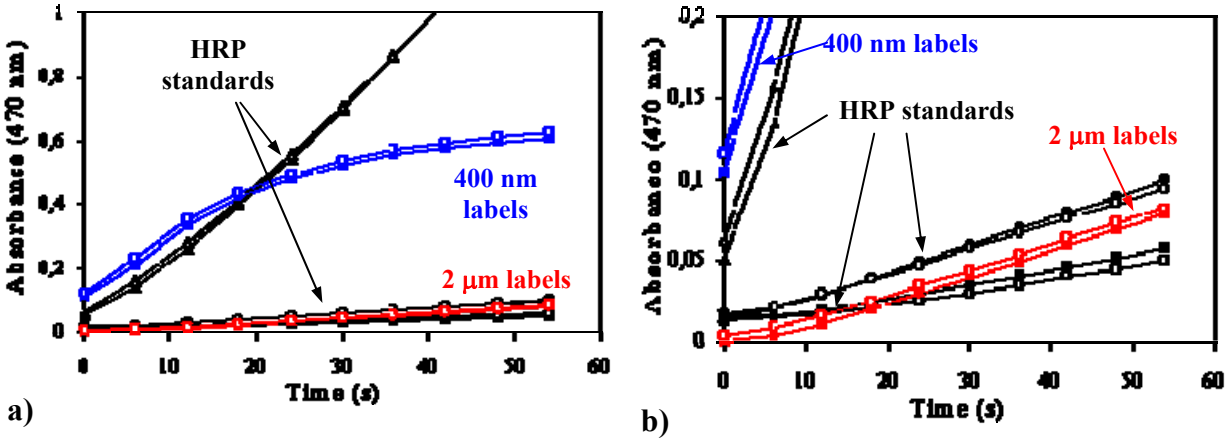

Fig. 3.5: a) Absorption measurements at 470nm for solutions with H_2O_2 and guaiacol with different HRP concentrations and with 400nm and 2µm labels with immobilized HRP. b) Close-up of a) for low values of absorption.

The following assumptions were made: (i) the rate of product formation is proportional to the enzyme activity; (ii) the activity of the immobilized enzyme is proportional to the activity of the free enzyme and (iii) the enzyme preparation is pure. Then the amount of active HRP immobilized to particles or microspheres was determined by comparison of the rates with the known HRP solutions. This provides a quantity of HRP for a given volume and weight of particles. The weight of HRP per particle is then calculated by dividing by the number of particles in the sample (company data). The weight of HRP per particle is then converted to the number of molecules using Avogadro´s Number and the molecular weight of HRP (44.000Da). Using this approach it was found that the immobilized enzymes remained active and that there were ~20 active enzymes per 2µm microsphere and ~40 active enzymes per 400nm particle. Taking into account the respective particle and bead dimensions one sees that there are much more active enzymes per unit area for the 400nm particles than for the 2µm microspheres, perhaps indicating a more dense surface functionalization in the former than in the latter.

3.2 Surface immobilization

The biochemical surface functionalization of the beads enables the immobilization of the particles to a substrate surface. This is an important aspect of

the on-going experiments: the detection of biomolecular recognition, as will be discussed.

The possibility of immobilizing different biomolecules to particles and beads has already been discussed. For the purposes of demonstrating molecular recognition was chosen a model protein called streptavidin. This has a tetrameric structure with a molecular weight of 60.000Da ([22]) and binds to a smaller biomolecule called biotin with a high affinity (~200-250pN) ([23], [24], [25]). Biotin can be found in many living systems where it plays the part of co-factor/vitamin (B12) ([26]). The strategy used involves the chemical binding of biotin to the spin valve sensor surface and the subsequent biological binding of a streptavidin functionalized magnetic particle to the sensor bound biotin. Fig. 3.6a shows a scheme for the streptavidin-biotin structural binding and Fig. 3.6b shows the structure of biotin. Particles with streptavidin immobilized to their surface were purchased directly from Micromod.

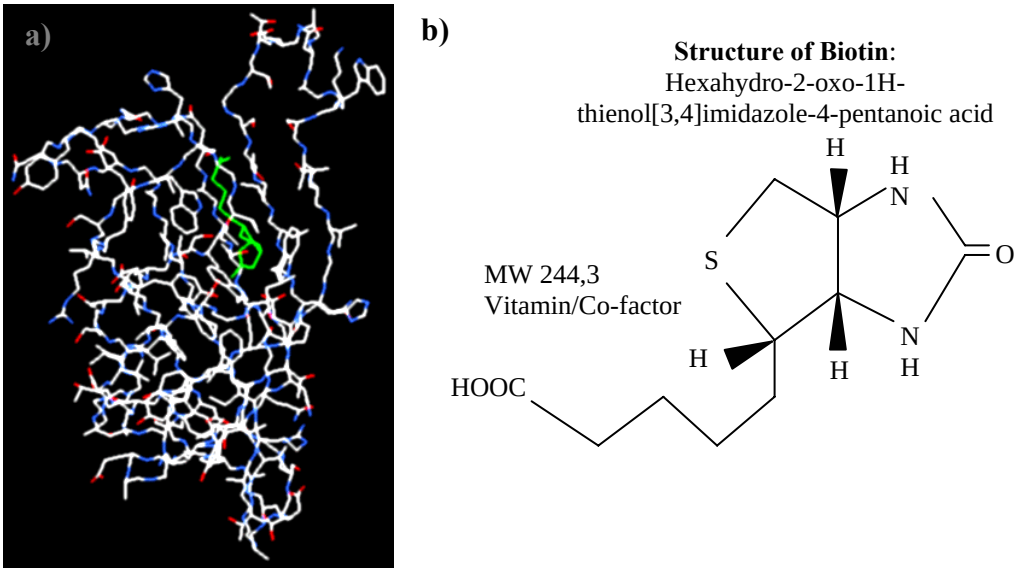

Fig. 3.6: a) Tridimensional scheme of the streptavidin-biotin biotin (biotin seen as green). b) Structure of biotion.

Prior to trying to bind particles directly to the sensor surface we tested the binding of particles to different substrate surfaces such as glass, SiO_2 and certain nitrides (aluminium, silicon and titanium tungsten). We also tried binding to progressively smaller areas. The protocol for immobilizing the particles to a substrate surface proceeds via the activation of the surface with APTS (3-aminopropyltrietoxy silane $C_9H_{23}NO_3Si$) to produce free amino groups. This is then followed by treatment with a biotinylated cross-linker (sulfosuccinimidyl-6-(biotinamido)-hexanoate or Sulfo-NHS-LC-Biotin) (Fig. 3.7), which binds biotin to the amino groups on the surface, and finally the introduction of the streptavidin functionalized particles. The binding is confirmed by water rinsing the substrate and verifying the presence of the beads. These procedures are illustrated in Fig. 3.8 and their details are described in Appendix A.

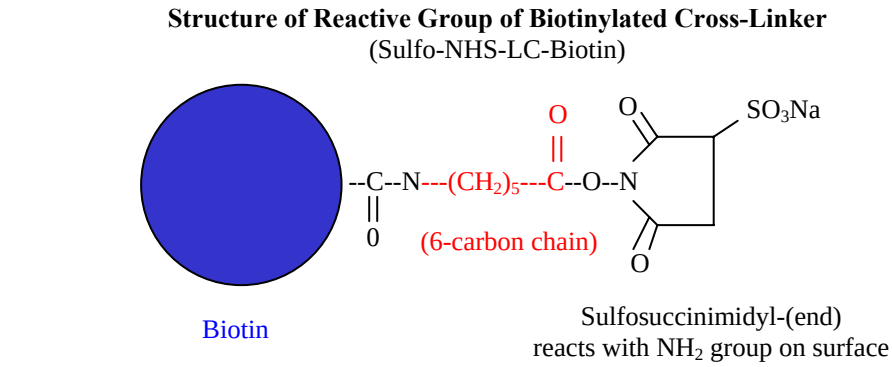

Fig. 3.7: Structure of the cross-linker bound to biotin.

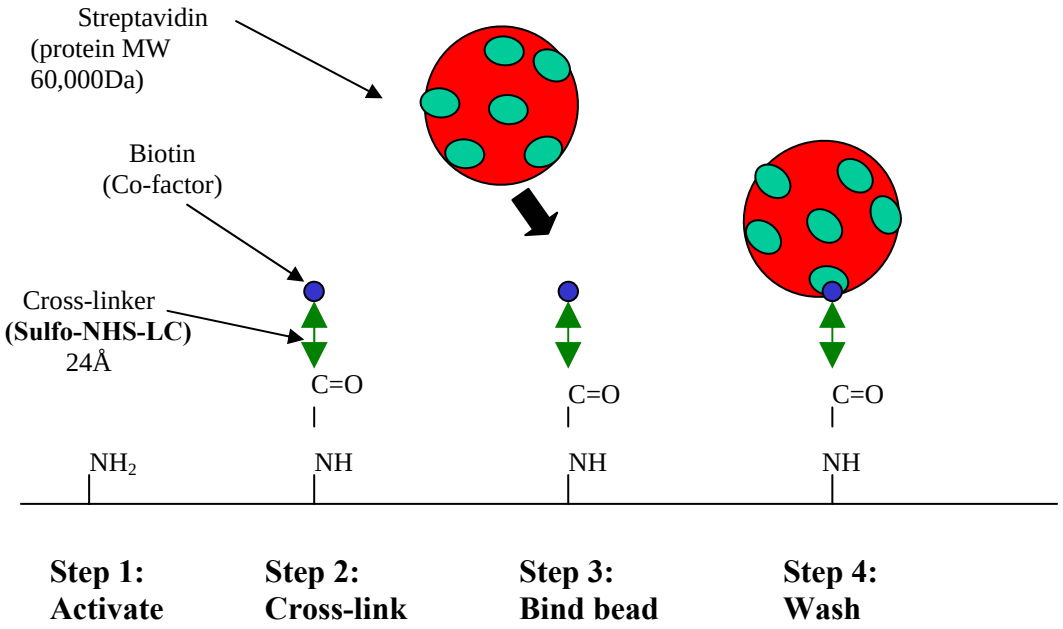

Fig. 3.8: Schematics of the protocol for immobilizing streptavidin beads on a substrate's surface.

In order to test the binding to different sized substrate surface areas a photoresist (PR+) mask was designed. This was deposited on the substrate before the binding procedure and removed afterward by treating the substrate with either acetone or Microstrip®2001. Using this approach arrays of particles with several sizes: 400×400, 200×200, 100×100, 50×50, 25×25 and 10×10 μm^2 were produced, as can be seen in Fig. 3.9 (for details about masking, PR+ and Microstrip®2001 see section 4.2 and check Appendix A).

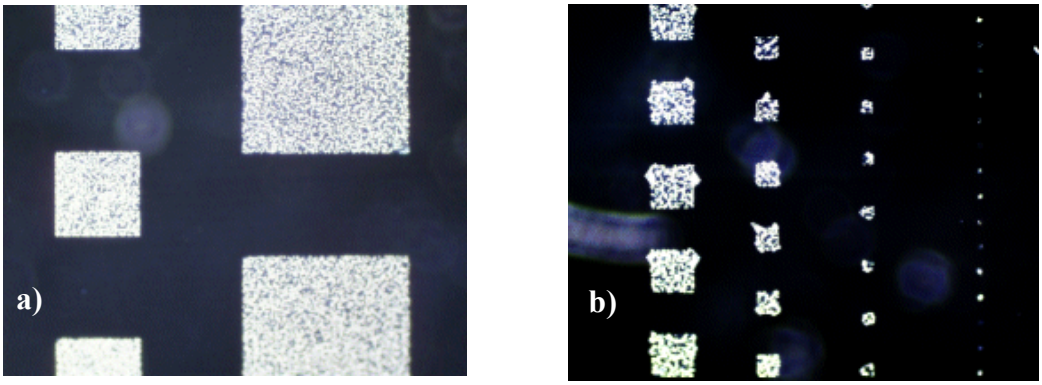

Fig. 3.9: Arrays of 2μm beads in a glass substrate: 400×400 and 200×200μm^2 a), and 100×100, 50×50, 25×25 and 10×10μm^2 b).

4. The Circuit

To achieve the proposed project goals a number of microchip circuits were devised. In this chapter all the steps for fabricating the microchip are presented, including chip design, processing and mounting in a suitable format for experimentation.

4.1 Design

The two main structural features of the chip are the spin valve sensors, which require contact connections for reading and the current line structures. The current line design was optimised with respect to the way in which the line could be used to control the movement and positioning of the magnetic particles. Four of the structures developed are shown in Fig. 4.1. The first three a)-c) were designed during preliminary studies, which included coursework in Microtechnologies: "Nano-magnetic Particles" ([27]) and the final design d) was the one used in this work.

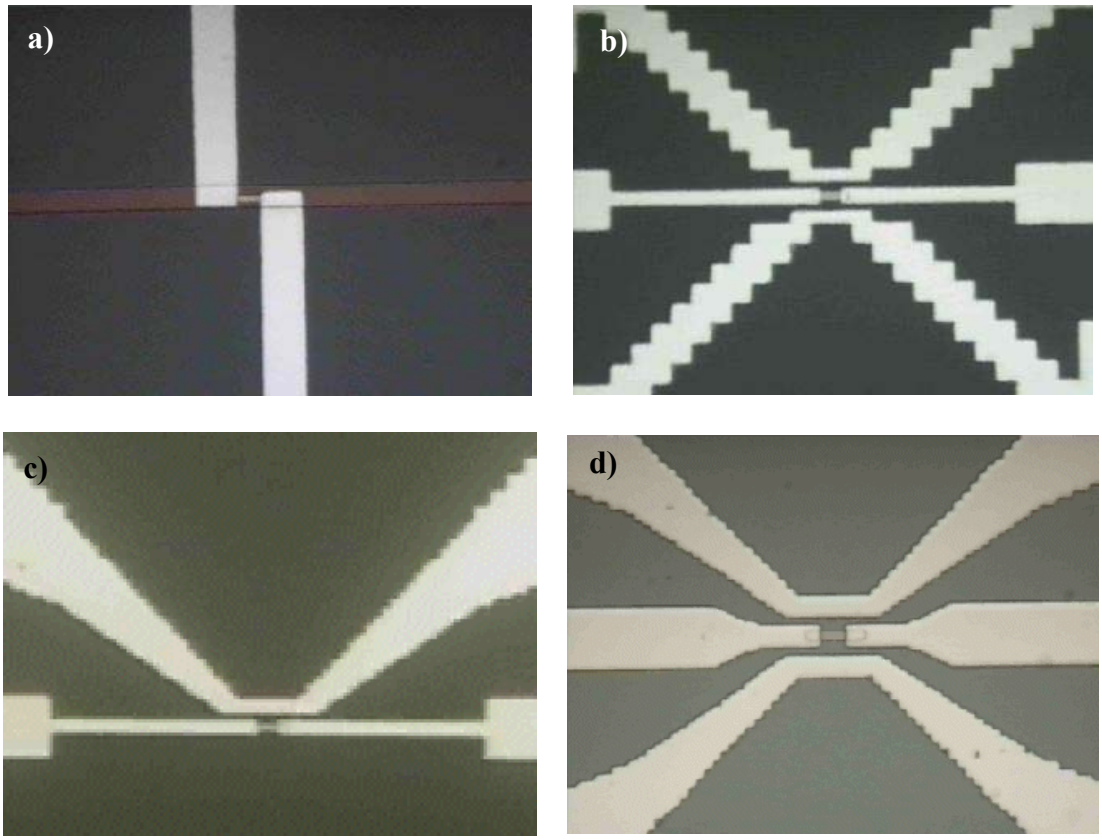

Fig. 4.1: Biochip's former designs: a) "Nanomag", b) "Biosensor", c) "Snsdiver"; and actual design: d) "Spider".

An initial design (not shown) "Micróbio" consisted of a simple straight current line, which had a section of narrower diameter in the central region. This was constructed by Filipa Brígido (a physics colleague on the Microtechnologies course) and proved the principle that a current line could generate sufficient field to attract the magnetic particles. Furthermore, it showed that the field generated was higher were the current line was narrower, due to higher current density.

The first design (Fig.4.1a), “Nanomag” ([27]), had a current line with four spin-valve sensors on top, which confirmed the attraction of particles to a sensor area, but also showed some potential problems: the 400nm dextran particles were found to stick to the lines and also to other parts of the chip such as wire bonded areas. This caused rapid fouling of the chip and lead to corrosion.

The second design (Fig. 4.1b) “Biosensor” ([28]) was made by the author and a Belgian Summer student from Katholieke Universiteit Leuven and from IMEC (Interuniversitair Micro-Elektronica Centrum), Roel Speetjens-Wirix, who was also responsible for its processing. This design was more useful for the movement of particles, but still showed some disadvantages. The staggered current lines, which became thinner near the sensor, were made with the purpose of concentrating particles near the sensor area, however, particles tended to become fixed in the steps (corner areas) of the lines. These current lines were also shared i.e. each current line had a staggered structure near two sensors. Consequently, two sensor areas were potentially fouled by particles during one experiment.

The third design (Fig. 4.1c), “Snsdiver” included tapered current lines i.e. narrowing more gradually, without large steps in the line structure. This was found to be much more successful in controlling the movement of the particles and was used to demonstrate that we could move particles to and from the sensor with ease. Originally this chip was designed with the intention of dipping the chip vertically into the particle solution. However, sensing experiments were not performed this way as problems were envisaged with the deposition of particles in the solution (away from the chip) and the difficulties in applying an external field.

Finally, the fourth design, the “Spider” design (Fig. 4.1d) was fabricated with the same tapered current lines structures, but having two associated current lines per sensor instead of one. This enabled us to move particles to and from the sensor from both sides and to use both lines simultaneously to saturate the sensor area with particles. The detection of both magnetic particles and microspheres was successfully accomplished successfully with this chip.

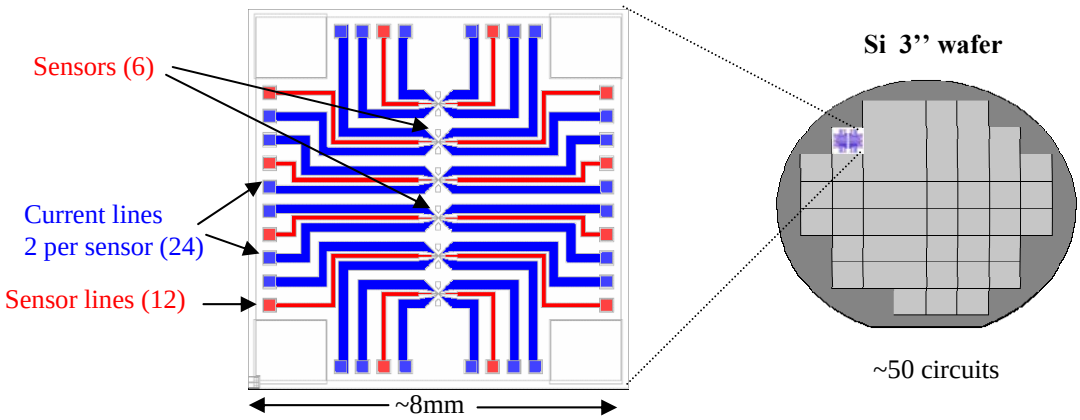

Fig. 4.2: The “Spider” layout design, where the sensor lines are shown in red and the associated current lines in blue and the sensors are located in the chip’s central region. There are ~50 chips per 3” wafer.

The layout of the "Spider" chip is presented in Fig. 4.2: each chip has 6 spin-valve sensors; each with 2 contacts (sensor lines) and 2 associated current lines, giving a total of 36 contacts. The chip area is 8×8mm^2 allowing for ~50 circuits to be made on a 3" Si wafer.

One can see in more detail the sensor and current lines structures in the following picture Fig. 4.3. As noticed the sensor is 2×6μm^2 and the sensing area, the area to concentrate the particles is ~20×20μm^2.

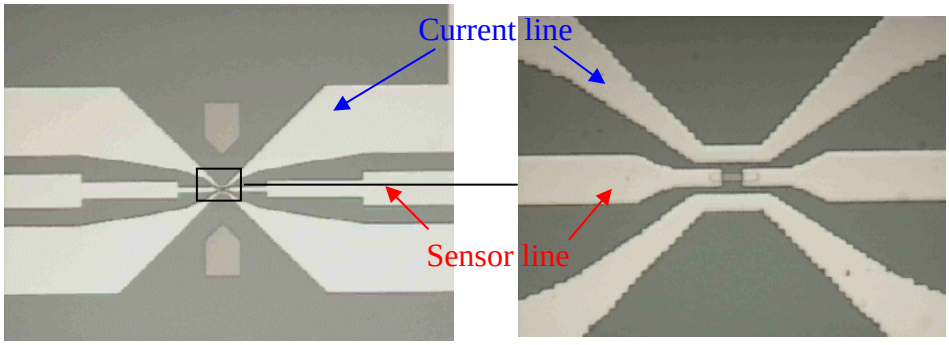

Fig. 4.3: Enlargement of the sensor region of the "Spider" layout and a further close-up of that region.

4.2 Processing

The dimensions of the chip structures are so small (e.g. a spin valve sensor is only a little larger and a lot thinner than a bacterium), that the fabrication processes must be performed very carefully and in a controlled environment. In particular, extra care must be taken to exclude dust. Consequently, the processing of these microcircuits was performed in INESC's clean-room facilities (Fig. 4.4). The clean-room comprises areas classified as 100 and 10, referring to the maximum number of dust particles per cubic centimetre of air in that region. This helps to assure the quality and reproducibility of the process.

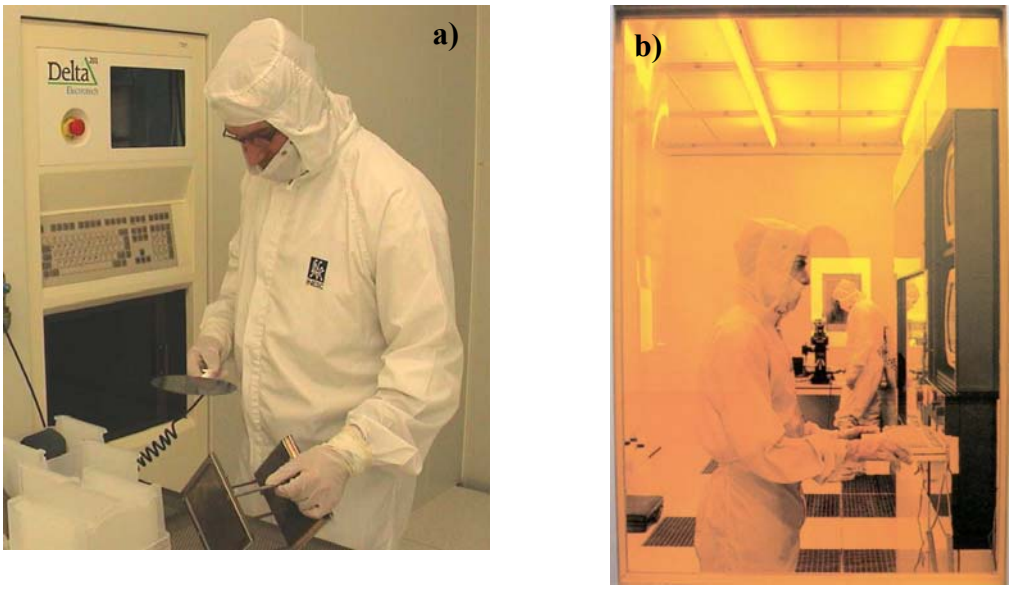

Fig. 4.4: Clean-room facilities: a) detail on clean-room garments; b) yellow room for circuit masking.

All the processing was done in the clean-room and is exposed in the run-sheets of two spider samples (samples #1 and #2) in Appendix B and schematically, as cross-sections drawings of the sensor and current lines, in Appendix C. The process is comprised by 20 steps, which are going to be discussed briefly below. This discussion should be accompanied by the mentioned appendixes for better understanding.

- **STEP 1:** Substrate Cleaning in Wet Bench
  In this step, a 3" Si wafer is washed with IPA (isopropyl alcohol) and rinsed with DI (deionised) water for removing any grease and/or particles from the substrate surface. For helping this washing one can use also clean-room paper embedded in IPA. After the washing, one blow-dries the sample with a nitrogen gun and then one heats the substrate in an oven at 130ºC for 30' for removing all remaining water.

- **STEP 2:** Spin-valve test Deposition
  Before the deposition of the spin-valve material in the substrate, a small strip glass sample is deposited for checking the properties of the material in a proper setup. The spider sample #1 test sample was deposited in Nordiko 2000 – a sputtering machine, while the spider sample #2 was deposited in Nordiko 3000 – an ion-beam deposition system ([17]). The deposition of the spin-valve material is the only difference between the processes of the two samples. So, in this way the thicknesses of the layers in the spin-valve structure are different as seen in the run-sheets (Appendix B). After the conclusion of both processes it was verified the better quality of the spider sample #2, thus all subsequent experiment were done with this microchips, so the spin-valve structure presented in section 2.1.2 is the one from sample #2. In spite of this, is presented below (Fig. 4.5), as an example, the transfer-curve of the spin-valve (bulk) test sample of spider #1 sample.

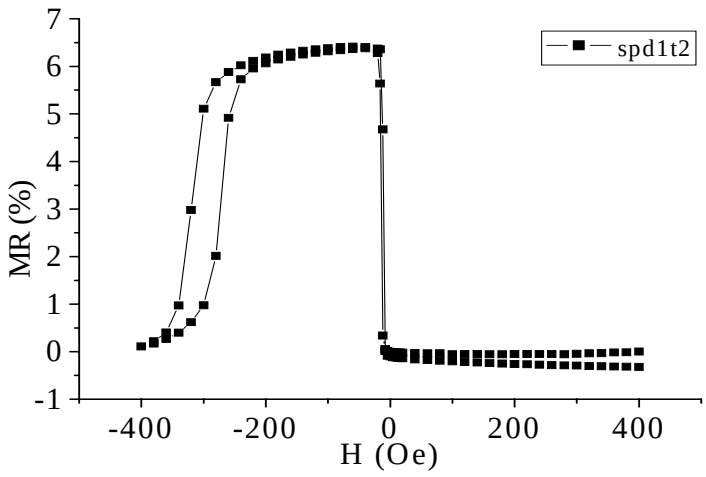

Fig. 4.5: Typical transfer-curve of a bulk spin-valve sample.

The spin-valve test samples are repeated until the characteristics of the bulk material are the required ones, namely: the MR (magnetoresistance ratio – eq. 2.1) signal ≥6%, the coercive field $H_c \leq 6Oe$ and the exchange field $H_{ex} \geq 250Oe$.

- **STEP 3:** Spin-valve Deposition
  After the right conditions for the deposition are obtained, the spin-valve material is finally deposited over the cleaned Si substrate.

- **STEP 4:** TiW(N_2) 150Å Deposition in Nordiko 7000
  In this step a TiW(N_2) 150Å layer is deposited over the spin-valve material. This layer protected the spin-valve material from corrosion and damage, besides acting as anti-reflective layer useful for a better mask exposure (see below). The titanium-tungsten nitrate layer is deposited in a sputtering machine: Nordiko 7000, present in the INESC's clean-room.

- **STEP 5:** Resist Coating (PR+) in SVG tracks
  For patterning the spin-valve sensor and thus defining its geometry is necessary to create a mask with the shape required, which is present in the spider layout. The drawn layout is composed of several layers, each one corresponds to a mask that will be used on the several steps of the processing. The layout program layer is first converted into a laser machine language. The laser will then draw the mask in a photo-resistive material (PR). This one is of organic nature and when exposed to light hardens (thus the denomination PR+). In this case the TiW(N_2) layer is coated with PR in a special track. As a note the PR coated layer has a 1.5μm thickness.

- **STEP 6:** Mask Exposure in DWL (spin-valve sensor definition)
  The PR layer is exposed by a 422 nm laser (near UV light), thus creating the required pattern (the mask). In this step the sensor shape is exposed as present in the chip layout. This chip layout exposure is repeated all-over the substrate surface (now the TiW(N_2) layer) according to a map as in Fig. 4.3, check also appendixes A for details.

- **STEP 7:** Mask Development in SVG tracks
  After the last step the PR layer became hardened where the laser light exposed it. Then the sample is developed in a track parallel to the coating one. These tracks are present in a yellow room (so the light doesn't harden the PR) inside the clean-room facilities. After the development one obtains a mask of PR with the sensors patterns. Notice, that the masking procedures are analogous to the photographic systems: a photosensitive film, the exposure to light and the developing.

- **STEP 8:** Spin-valve + TiW(N_2) Etch in Nordiko 3000
  The spin-valve sensor structure is, finally, obtained by the "eating away" the material through the mask, in a process called etch. The material of the sample: Si/Spin-valve material/TiW(N_2) which is not protected by the PR mask will be etched away by an ion milling process in Nordiko 3000 machine, leaving the sensor shape structures well defined.

- **STEP 9:** Resist Stripping in Wet Bench
  After the last step it's necessary to remove the remaining PR material on top of sensor structure (check Appendix C). This is done by putting the sample on a solution (a special compound for removing the photoresist) at 80ºC, for the necessary time, and, eventually, applying ultrasounds that make the PR

removal easier. After this the sample is washed with IPA and then rinsed with DI water, this is necessary because the Microstrip®2001 solution when in contact with water becomes corrosive for the circuit. After rinsing the sample is blown dried with a nitrogen gun. In the end of all this steps the circuit will appear as exposed in Appendix C - spin-valve sensor definition, in a optical microscope observation. Notice the existence of some "arrow" pads that are used exclusively for pointing the position of the sensors, which due to their small size ($2\times6\mu m^2$) are difficult to find under the optical microscope.

- **STEP 10:** Resist Coating (PR+) in SVG tracks
  In this step starts the definition of the sensor lines (sensor contacts) and the associated current lines. For that one first defines the mask over the sample by coating it with PR, as in STEP 5.

- **STEP 11:** Mask Exposure in DWL (sensor lines and current lines definitions)
  The PR coating is away exposed but this time with a different layout layer (see run-sheets in Appendix B), for making the required mask.

- **STEP 12:** Mask Development in SVG tracks
  The sample is the developed in the SVG developer track as in STEP 7, remaining the hardened PR mask.

- **STEP 13:** Al 5000Å Deposition in Nordiko 7000
  In this step 5000Å of Aluminium are deposited over the PR mask. The Al will be the metal contacts for the sensors and at the same time the associated current lines for attracting the particles near the sensor. The Al is deposited in the Nordiko 7000 machine.

- **STEP 14:** Al Liftoff in Wet Bench
  To obtain the required structures for the sensor and current lines one needs to remove the material on top of the mask. In this way, the structures that remain are the ones that don't have PR. This is done by putting the sample in a Microstrip®2001 solution, to remove the PR and the material over it. This procedure is called Liftoff and like in resist stripping, one frequently apply ultrasounds to facilitate the PR removal. The STEPS 10 to 14 are schematically exposed in Appendix C – sensor lines and current lines definitions. In this schemes can be seen a cross-section of the sensor and of the sensor and current lines (in small), while in Appendix C – spin-valve sensor definition, only the cross-section of the sensor was seen. In the end of STEP 14, the structures obtained can be seen in the Appendix referred, with some dimensions present.
  At this time, the characteristic transfer-curve of the sensors, as in Fig. 2.5, can be obtained with a proper experimental setup present in the Centre of Microsystems and Nanotechnologies group, to check whether or not the sensor work properly and decide to continue or not the running process.

- **STEP 15:** SiO_2 3000Å Deposition in Alcatel SCM 450
  One deposits now 3000Å of SiO_2 (silicon dioxide) on the sample for protecting it against corrosion and damage. The deposition is done in the Alcatel SCM 450 machine – a sputtering device.

- **STEP 16:** Resist Coating (PR+) in SVG tracks
  The deposition of the protecting oxide is all-over the sample's surface, thus the contacts for the sensor and current lines are covered by oxide. It's then necessary to open the vias through the oxide, so another mask is needed. As before a PR layer is coated on top of the sample in the SVG coating track.

- **STEP 17:** Mask Exposure in DWL (opening contact vias)
  The mask is then exposed with the laser as before.

- **STEP 18:** Mask Development in SVG tracks
  The development follows as expected to leave the required mask over the sample.

- **STEP 19:** SiO_2 Etch in LAM
  To open the vias over the sensor and current lines pads one will etch the sample (the material without PR over it will be "eaten" away). The etch is done by a LAM machine and is called a reactive ion etch since it uses, besides the ion's physical etch, chemical etch with O_2 and CF_4 (see Appendix B).

- **STEP 20:** Resist Stripping in Wet Bench
  After the etch is done, is now necessary to remove the remaining PR in the same way as seen above. With this step the process of manufacturing is now completed. The pictures obtained in the end of the process are shown in Appendix C – passivation and opening contact vias, along with some dimensions of the structures. As a note, in this latter Appendix B section, only the first scheme in the STEP 15 presents cross-section views of the sensor and sensor contacts and current lines, all the following STEPS show only the sensor and current lines cross-section views, as one only need to open the contact vias.

Worthy of mentioning is that the exposed process takes in total around 2 weeks to finish, if every step works out OK!

At the end of the process one obtain a 3" Si wafer with ~50 circuits, each one with 6 spin-valve sensors, making ~300 sensors total. As one wants to use each circuit individually one used a dicing saw to separate them (see Fig. 4.6).

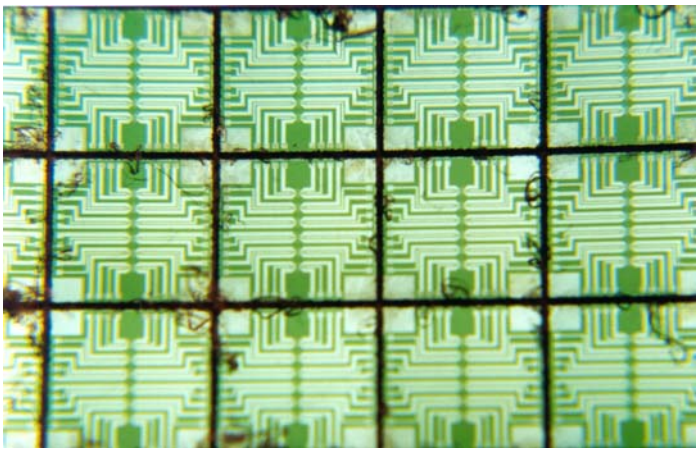

Fig. 4.6: Final manufactured chips cut with a dicing saw.

As a fun way to compare the circuits' dimensions to familiar objects the following picture (Fig. 4.7) is presented.

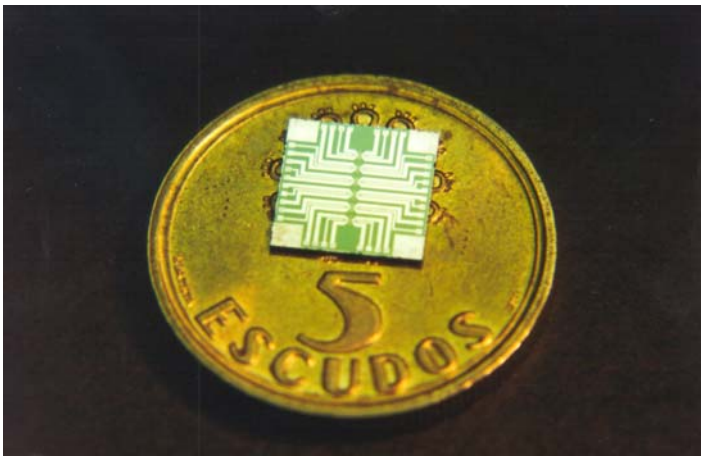

Fig. 4.7: A fun comparison of a biochip to a 5 escudos coin.

4.3 Mounting

After the processing and dicing of the chips, each one was mounted on a chip carrier, which is a holder for the chip with 40 contacts (remind that the "spider" chip has 36 contacts). Since the chips' contact pads are quite small ($200\times200\mu m^2$), it's not possible to make the electrical connections between the chips' contacts and the chip carrier's contacts the traditional soldering way. The referred liaisons were made by a thin Al wire in a process called wire bonding, which uses ultrasonic vibrations to bind the Al wire to a metal contact of the chip or of its holder. This mounting in the chip holder makes the measurements and experiments much easier to perform. See in Fig. 4.8 a chip mounted in a 40 pins chip carrier.

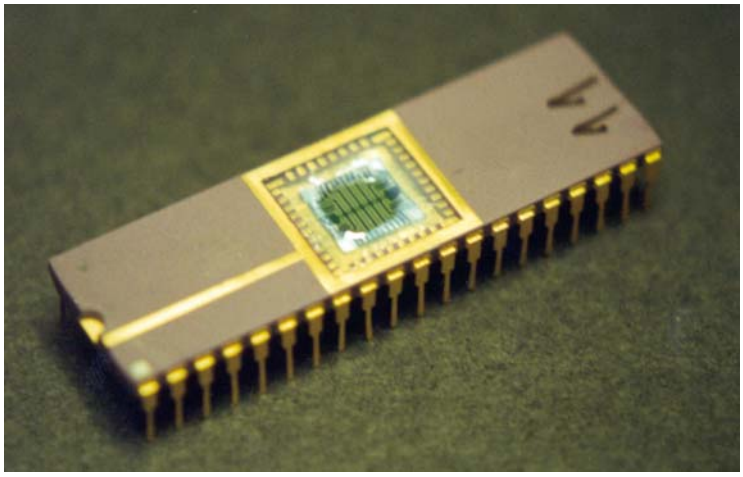

Fig. 4.8: Chip mounted in a 40 pins chip carrier.

The movement and detection experiments were performed in an aqueous solution containing the magnetic particles, which was applied to the surface of the chip (section 4.1). In order to prevent the fouling and corrosion of delicate contact areas (as had happened previously), the wire bonding was covered with a silicon gel. This was applied as a soft gel, which was allowed to harden by drying for a period of 3-4 hours at room temperature, prior to the use of the chip. (see Fig. 4.9).

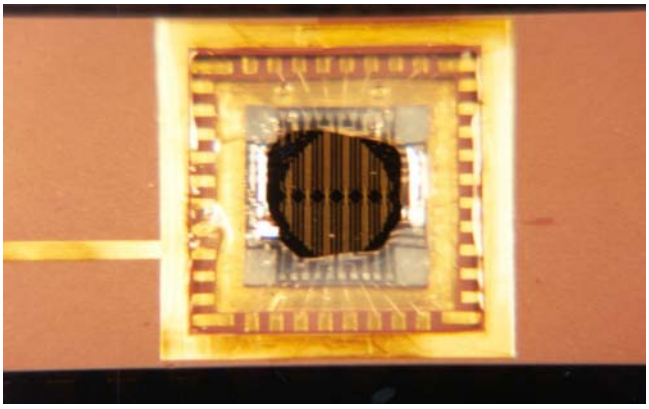

Fig. 4.9: Picture showing chips' contacts wire-bonding and contacts' protection with silicon gel.

5. The Experiments

The structural integrity of the current lines and sensors were checked electrically prior to the use of a chip in an experiment. A current was passed through each line sequentially to assure that the lines or sensors had not been damaged during the processing or wire bonding steps. Also the resistance of all the sensors was measured and compared with the initial measurements made after their fabrication. Once the performance of the current lines was assured and the response of the sensors confirmed the chips were passed for experimentation.

In this chapter, it the experimental setup that was developed will be described and some of the results will be discussed, including the behaviour of the particles in a magnetic field, the controlled movement and positioning of the particles and their detection. A simulation made for the expected signal a magnetic particle would generate in the spin-valve sensor is also presented. Finally, some of the on-going experiments will be considered.

5.1 Experimental setup

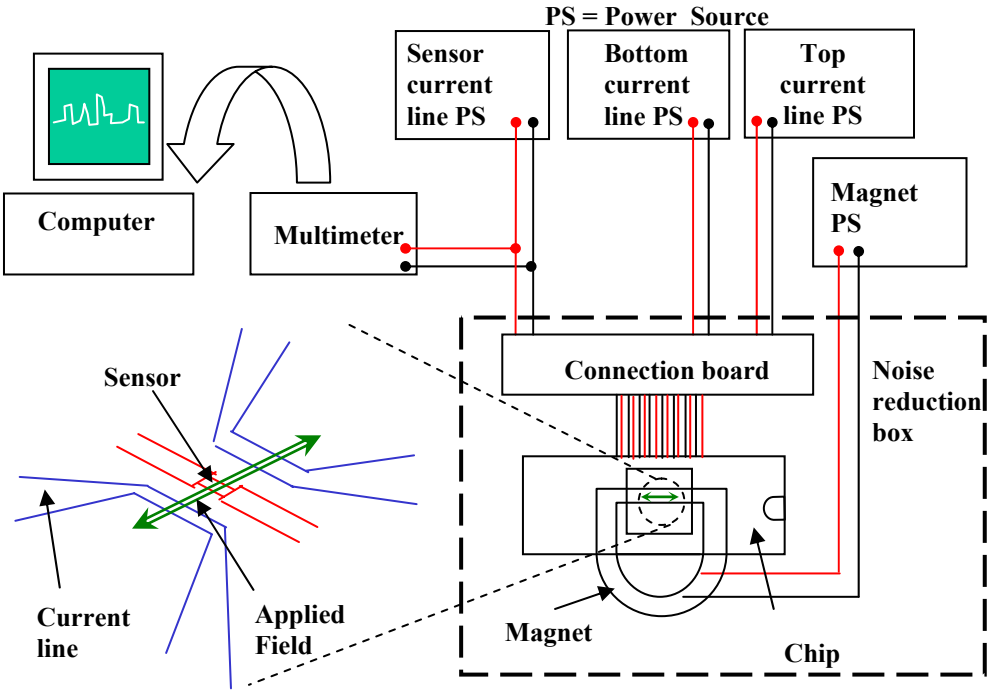

Fig. 5.1: Experimental setup used in the presented work.

For experimental purposes the chip carrier was mounted in a support, which had 40 large pins corresponding to the 40 chip holder pins. This allowed the connection to the chip more readily to other devices. The support connections were made inside a homemade electrostatic noise-reduction box connected to power sources for the sensor and current lines. The sensor lines cables are also connected to a multimeter for making voltage readings of the sensors. These voltage readings change when the sensor's electrical resistance changes due to a magnetic field. The multimeter was then connected to a GPIB board inside a computer, and a VISUAL

BASIC program (biosensor.vbp) was used to collect the board's data as ascii files. In the setup there is also a power source for an electromagnet that creates the field necessary to magnetize the superparamagnetic beads (see section 2.3). As a note, all cables used are BNC to further reduce noise. This experimental setup is presented above in Fig. 5.1 as well as the direction of the applied field relative to the sensor orientation, as it will be discussed in the next section.

The first detection experiments (see section 5.4.2) were made with this setup. But, in subsequent experiments it was necessary to visualize the particles at the same time as the voltage measurements were made. For that purpose the support of the chip holder was placed over the stage of a light microscope so that the sensors could be positioned beneath the objective lens. Nevertheless, the contacts for the power sources remained inside the noise-reduction box.

5.2 Bead alignment in magnetic field

The superparamagnetic particles only acquire a non-zero magnetic moment in the presence of an external magnetic field (section 2.3). An electromagnet was constructed for this purpose, which could be placed around the chip to generate an in-plane field (see Fig.5.2). The field generated with current was measured with a Hall probe using a Gaussmeter.

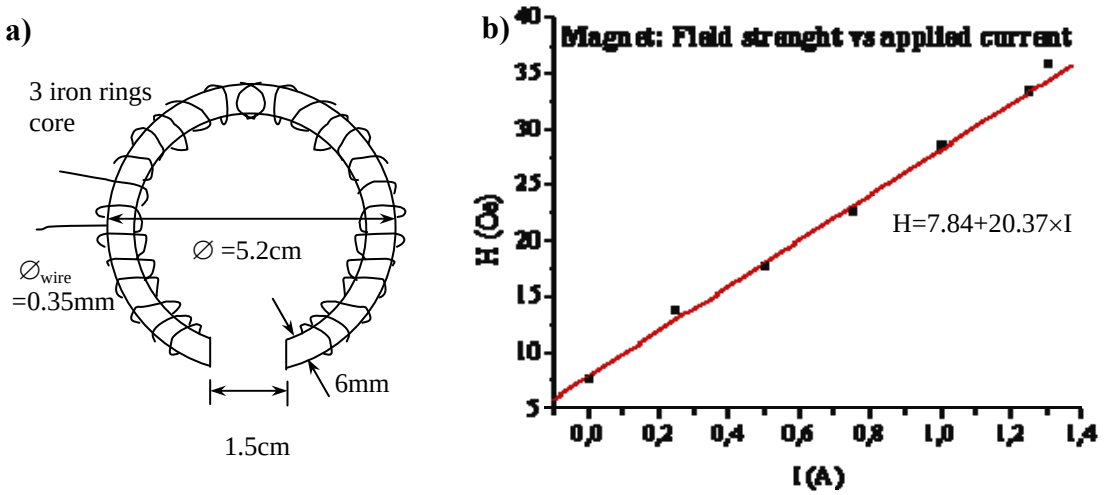

Fig. 5.2: a) Scheme of the electromagnet. b) Magnetic field generated by the electromagnet as a function of the applied current, as measured in the gap.

As before in Fig. 2.8, it was seen that the labels aligned in the direction of the applied field, forming rows (see Fig. 5.3 – work performed in "Snsdiver" chip).

The latter behaviour was useful for understanding how the particles arrange themselves and how they could be detected. In the following detection experiments it was shown that when the applied field was parallel to the width of the sensor (as in Fig. 2.4) the detection was not possible, but only when the applied field was in the direction of the easy magnetization – the height of the sensor – considerable voltage changes were measured. A third possibility for the direction of the applied field is perpendicular to the sensor, that is, perpendicular to the plane of the circuit. In this configuration the detection is also possible and initial saturation signal data was of a similar magnitude (this is presently being further investigated). However, all the data

presented was obtained using the configuration shown in Fig. 5.3b. Additionally, for all the experiments an external field value of ~15-20Oe was used, in part due to the capabilities of the magnet's power source and also because it was still in the linear range of response, as in Fig. 5.2. It was shown that this value of field was enough for magnetizing the beads and for successfully making the detection.

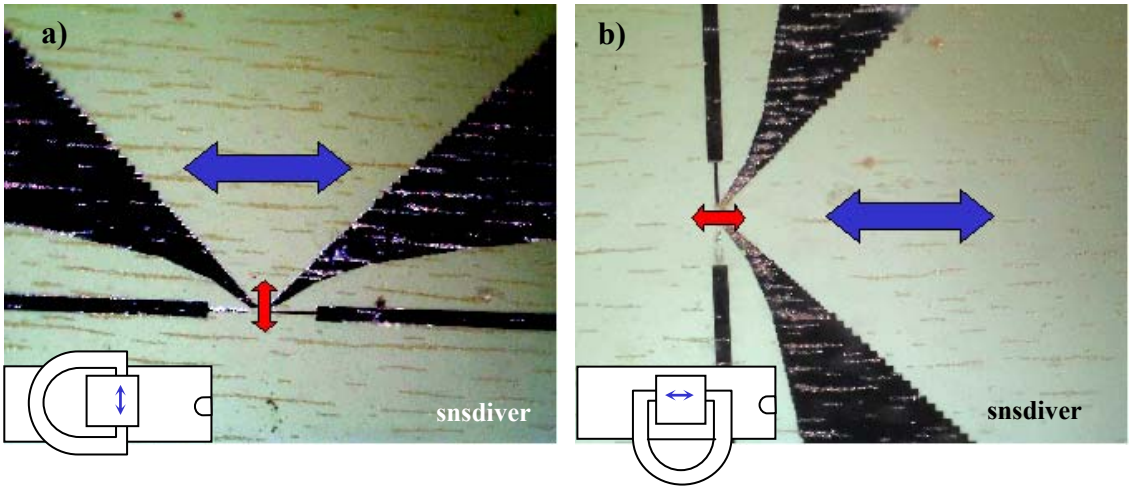

Fig. 5.3: Bead alignment in magnetic field: blue arrow – external applied field; red arrow – local field generated by current/sensor lines and direction of the sensor's pinned layer. The beads align in the direction of the applied field forming rows. a) External field perpendicular to sensor's height. b) External field parallel to sensor's height. Insets: orientation of the magnet relatively to the chip carrier.

5.3 Controlled movement

In section 2.2 it was mentioned that when an electrical current passes through a metal line a magnetic field is generated. This same magnetic field is sufficient to magnetize the particles and thus is able to attract them. So with the use of two current lines associated with each sensor we were able to control the particles movement by current modulation i.e. turning the lines on and off (passing or not current).

This methodology was also used to bring the particles near to the sensor, increasing our chances of detection. This was also far less time consuming than waiting for a particle to pass over or near the sensor as a result of random motion. The diameter of the tapered Al lines on the spider chip were reduced from 150μm to 5μm near the sensor (see Appendix C) and with these lines it was possible to successfully concentrate the particles near the sensor: from one single to several 2 μm particles were controllably placed near the sensor.

Fig. 5.4 shows some examples of the positioning of particles using current lines. Fig. 5.4a, b and c show that with current passing the bottom current line attracts more and more particles to an area close to the sensor, whilst Fig. 5.4d shows the effect of passing current through both lines. In these experiments it was found that a ~20mA current was sufficient to focus particles at either side of the sensor.

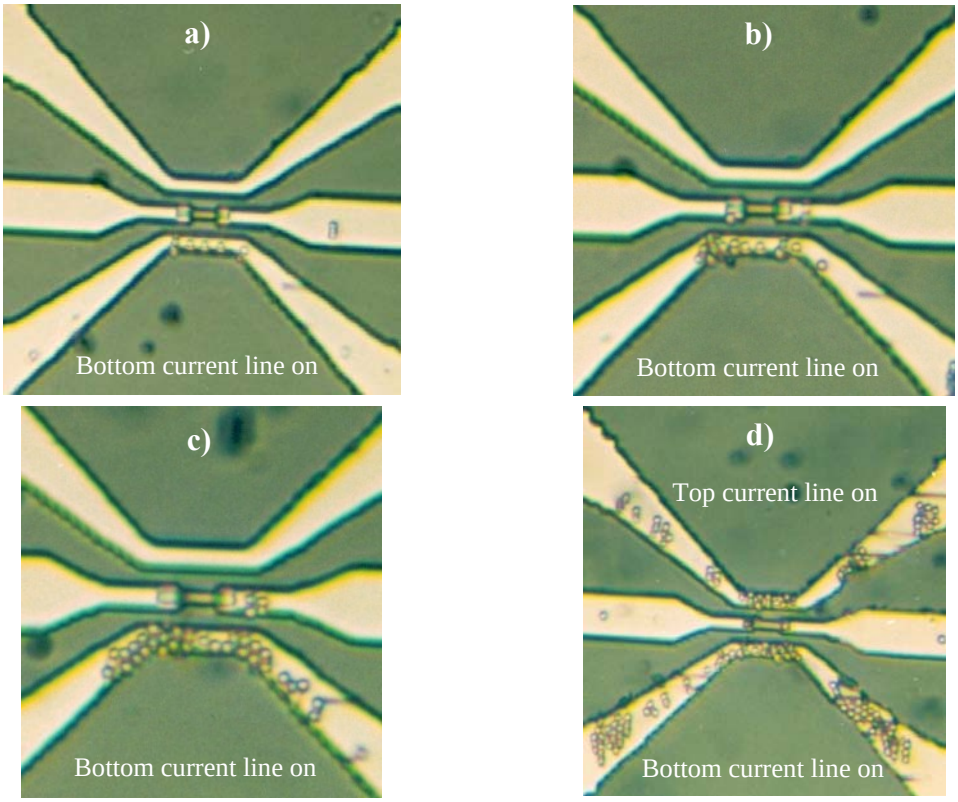

Fig. 5.4: Controlled bead placement in an area close to the sensor. a), b) and c), figures in function of time for the attraction of particles to the thinner region of the current line (bottom current line on). d) typical picture obtained when both current lines are left on for some time.

5.4 Detection

In this section, we will first discuss the expected signal a particle would generate and then focus on the detection experiments for the magnetic particles with or without immobilized biomolecules. Finally, we will discuss the on-going and future work.

5.4.1 Expected signal

To verify if the obtained measurements were the expected ones, a simple simulation was made with the software IDL 5.4. This simulation was only performed for one 2µm microsphere as they could be observed, moved and detected as single bodies. As discussed in section 2.3 the 400nm particles have the tendency to aggregate even at a zero applied field and, furthermore, being so small they are difficult to visualize independently (see Fig. 5.5a and b). In this way, the 2 µm microspheres were approximated to a magnetic dipole, with its centre at the geometric centre of the bead (a sphere). The magnetic field generated by the dipole at the position $\vec{r}$ from the centre of the dipole is translated by equation 5.1 in SI units ([18]).

$$B(\vec{r}) = \frac{\mu_0}{4\pi}\left(\frac{3\vec{r}\cdot(\vec{r}\cdot\vec{m})}{|\vec{r}|^5} - \frac{\vec{m}}{|\vec{r}|^3}\right) \qquad (5.1)$$

Where $\vec{m}$ is the dipole's moment. The external field is ~15Oe and is applied parallel to the height of the sensor as discussed in section 5.2. An external field of ~15Oe generates a particle moment of ~5×10^{-12}emu (or ~5×10^{-15}J/T), as seen in section 2.3.1.

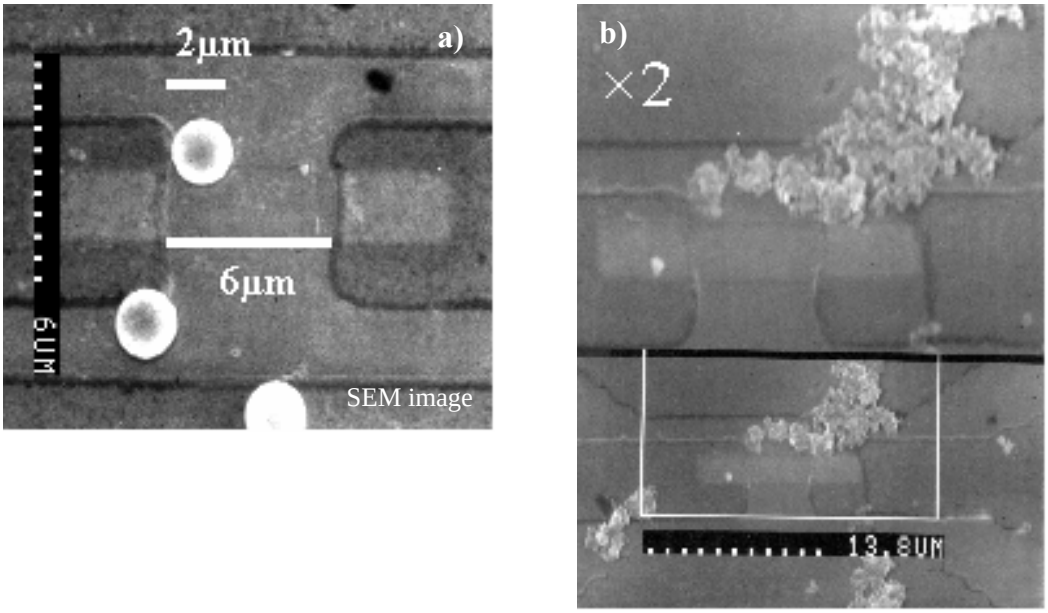

Fig. 5.5: Scanning Electron Microscope (SEM) images showing the spin-valve sensor and: the 2µm microspheres a); the 400nm particles b). Also in b) is shown in the upper part a 2× enlargement of the lower part of the image. Notice the clustering of the 400nm particles in b).

In the simulation the label is theoretically placed directly above the 3000Å oxide layer that protects the spin-valve sensor (and the 150Å TiW(N_2) layer), so the centre of the dipole is located ~1.3µm above the sensor layer (keeping in mind that the particles have a 2µm diameter), as seen in Fig. 5.6. As the thickness of the spin-valve sensor is so small (~208Å) compared with the distance of the dipole to the sensor, this latter was considered as a simple sheet in the simulation. This sheet was then divided in cells and the dipole field was calculated for each one of them.

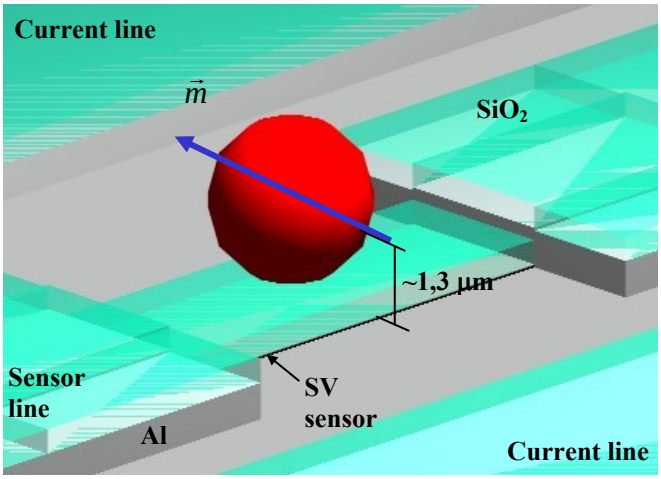

Fig. 5.6: 3D schematic of the 2µm location relatively to the sensor for the simulations of the expected signal.

The experimental conditions where considered in the simulation i.e. the sensor is considered biased with a current of ~8mA. Then it was calculated, in each cell, the change in direction of the magnetization, according to eq. 2.6 (Notice that, only components of the field in the direction of the pinned layer are significant – section 2.1.2). An average of all $\sin\theta_f$ is then taken over all cells and the voltage output due to a particle is obtained through eq. 2.5.

For the maximum estimate of the value to be obtained due to a single bead, several placements in respect to the sensor area were tried. It was shown that the maximum value was obtained when the microsphere is right in the geometrical centre of the sensor, as in Fig. 5.7. The field intensity and direction generated by the label on the sensor level is shown in Fig. 5.8 as a colour code: black, the most intense value of field in the direction opposite to the external field; white, the most intense value of field in the same direction of the applied field; and the shades of reds, the increasing values of field intensity.

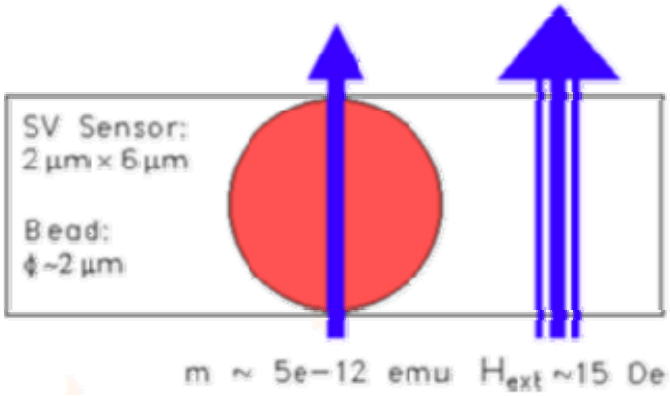

Fig. 5.7: Conditions for the maximum single-bead expected signal simulation: bead location, applied field (big arrow) and resulting moment (small arrow).

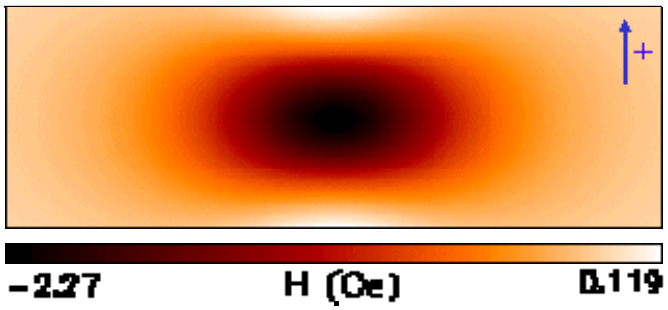

Fig. 5.8: Field intensity and direction generated by the 2µm magnetic label on the sensor level.

Using eq. 2.5, the maximum estimated value obtained for a single 2µm bead was ~400µV. In terms of the transfer-curve, as Fig. 2.5, with the biased sensor and a ~15Oe applied field, the change in response of the sensor is quite small, as seen in Fig. 5.9 in red. In this picture, comparing the output expression with eq. 2.5 we see that the resistance R is equal to $R_{sqr} \cdot W/h$, as is already known (R corresponds to the minimum resistance of the sensor).

Finally, with this simulation program it was also verified that when the applied field is parallel to the width of the sensor the detection is practically impossible. When

the external field is perpendicular to the sensor plane, although the detection is possible, the projected values are smaller.

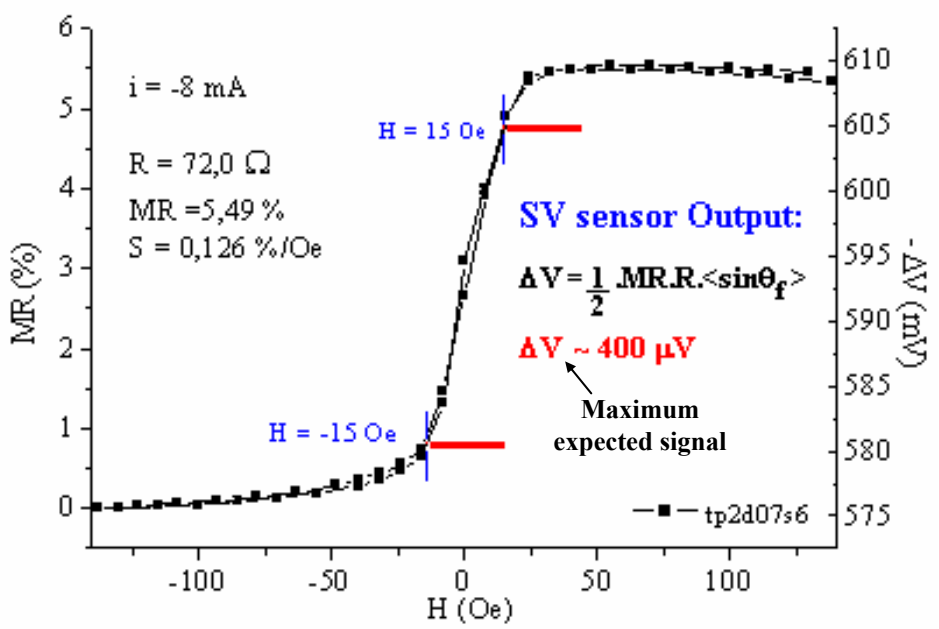

Fig. 5.9: Typical spin-valve sensor's transfer-curve, showing the operation point at ± 15Oe (blue lines) and the maximum expected change in signal due to a 2μm bead in the centre of the sensor and a distance of ~1.3μm from it (red bar).

5.4.2 Experimental detection

The detection experiments were made using a general procedure. First, the tapering lines were turned on (~20mA currents passing through) with the purpose of focusing the labels at sites (~5×15μm^2) near the sensor, as discussed in section 5.3. The current lines were then turned off and the beads were then seen to move to the top of the sensor and a simultaneous change in resistance was observed. The bead detection could be repeated by moving the labels to and from the sensor by switching the current lines on and off again as required. The background contribution or effect of current line changes on the sensor response was determined in control experiments performed without magnetic particles.

With this procedure both 400nm and 2μm labels were detected in bulk numbers (>>10). In the initial experiments the average MR signals at 5mA sense current were 0.3% (1.2mV) and 0.15% (0.6mV), respectively (the MR signal of the spin-valve sensors is ~5%). The observed saturation signals for Nanomag®-D were higher due to the smaller size and hence higher density of labels that can accumulate on the sensor's surface (recall to section 2.3.1).

Both types of labels with biomolecules immobilized on the surface (namely HRP – see section 3.1) were also detected. The signals obtained were the same as those obtained without biomolecules immobilized. As expected, the presence of biomolecules on the particles surface doesn't change the magnetic detection.

As previously mentioned in sections 2.3 and 5.4.1, the 400nm particles have the tendency to cluster forming larger magnetic bodies of unknown numbers of

smaller particles. This makes the determination of signals for single particles very difficult (using the stated experimental means). Consequently, all subsequent experiments were performed only using the 2μm microspheres. Fig. 5.10 below shows real-time detection signals for the 2μm labels with immobilized HRP molecules (~20 HRP enzymes remain active per label – see section 3.1.1).

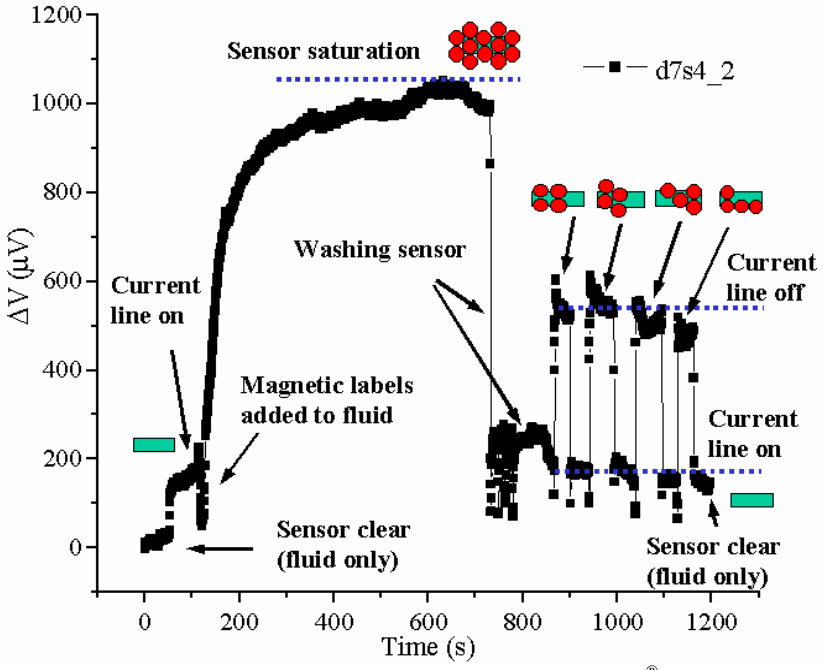

Fig. 5.10: Real-time data for the movement and detection of Micromer®-M labels with immobilized horseradish peroxidase. Shown also the relative position of the labels to the sensor.

Note that the green rectangle represents the spin-valve sensor and the red circles represent the Micromer®-M beads. A similar chart but with a different biomolecule immobilized – streptavidin – is shown in Fig. 5.11.

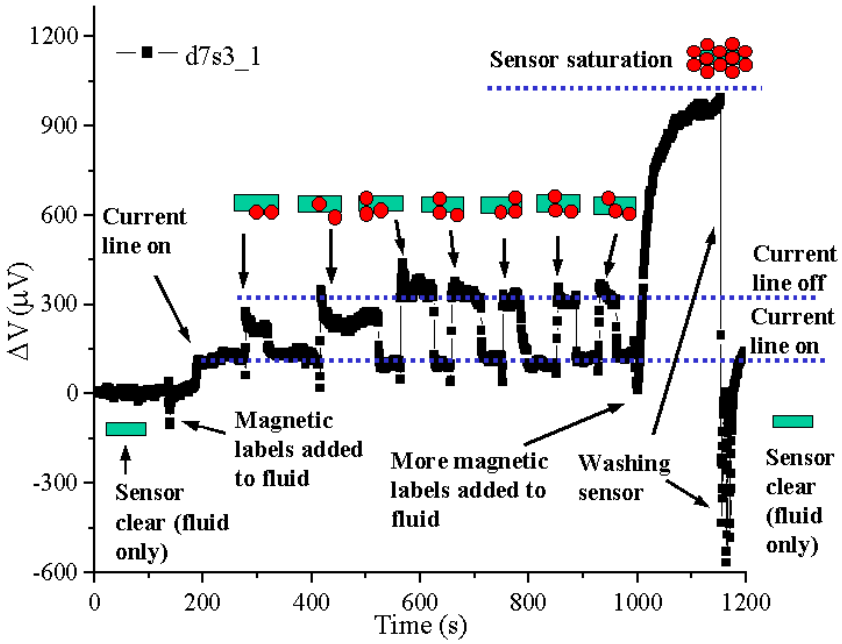

Fig. 5.11: Real-time data for the movement and detection of Micromer®-M labels with immobilized streptavidin. Shown, as before, the relative position of the labels to the sensor.

These latter plots and additional data were used to calculate average detection signals for 1-6 labels and saturation signals (>6 labels) for different sensors (see Fig. 5.12).

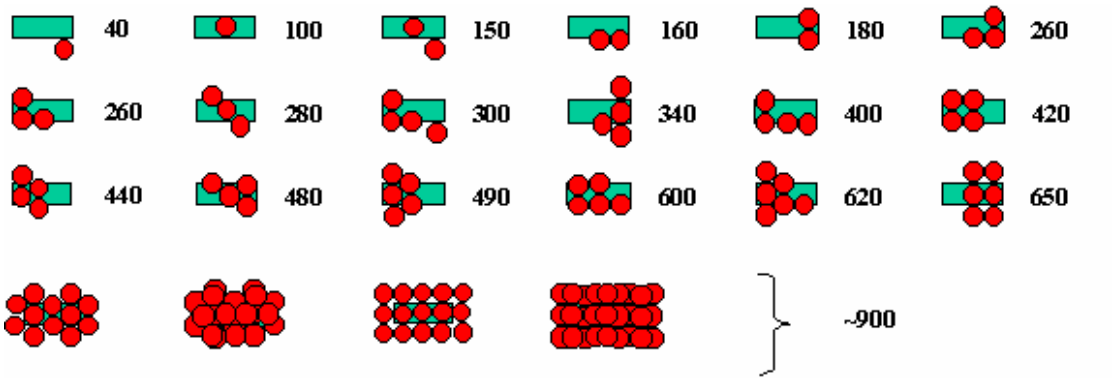

Fig. 5.12: Bead position vs sensor signals (μV) for 2μm beads and saturation signals.

Single labels gave a response in the order of 100μV with sensor saturation occurring around 1mV. The noise level was typically 10μV (1% saturation). As a note, turning one current line on (~20mA) produces a signal of up to 70μV. All these signals were found to be reproducible with respect to sensor and chip.

Remember that the maximum expected signal for a 2μm bead was ~400μV (see previous section), this is, around 4 times bigger the obtained signal ~100μV. The expected signal is reasonably close to the experimental signal, although there are several sources of any discrepancy e.g. the rather simplistic nature of the simulation, the fact that the effective magnetic moment of a single bead might be smaller (the field generated by the magnet in the exact plane of the chip may be smaller than the considered 15Oe, thus lowering the particles' moment or perhaps the bead is actually a greater distance from the sensing layer (via electrostatic repulsion).

5.4.3 Detection of biomolecular recognition

Presently, the streptavidin-biotin binding couple is being studied to enable simultaneous biological binding and signal detection i.e. the detection of biomolecular recognition. In pursuit of this goal a mask was defined over the sensor area where the biotin will bind using the procedure described in section 3.2. With only the sensor's surface biotinylated, streptavidin-immobilized particles (like the ones used for the plot in Fig. 5.11) should bind to the biotin and this will be accompanied by the signal. The bound bead will then no longer be moved back to the adjacent current line when a current is passed. In addition, washing the circuit's surface to reveal that the bead(s) remain in the sensor's area will then verify the effective streptavidin-biotin bond. A scheme for this process is illustrated in Fig. 5.13 below.

To remove the biotin bound streptavidin-immobilized particles, hopefully use free biotin might be possible. This has a higher affinity for streptavidin than the surface-bound biotin. In this case, the release of the streptavidin bead should also be detected by the spin-valve sensor.

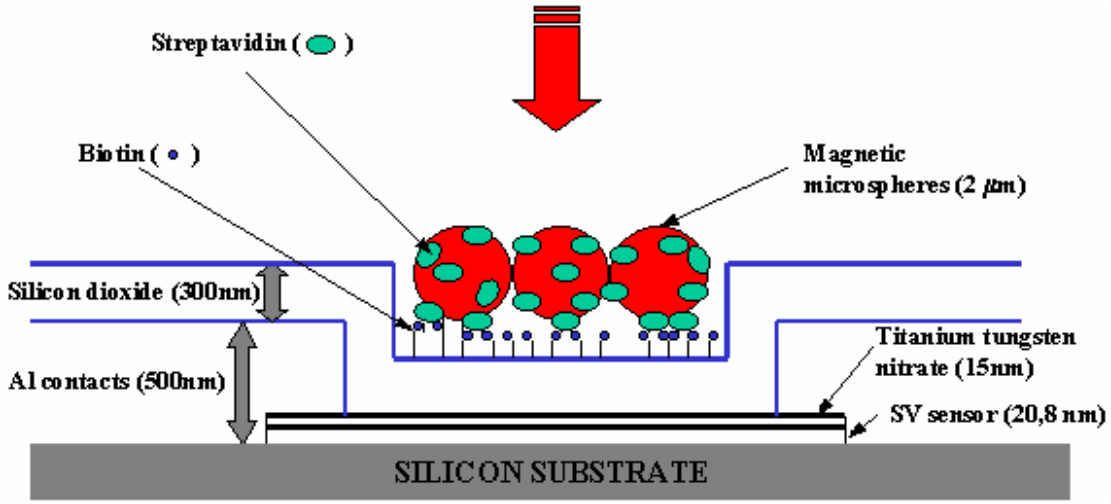

Fig. 5.13: Schematic of the streptavidin-biotin binding at the spin-valve sensor site.

In order to achieve this, several important steps have already been achieved. Arrays of 2μm particles of several area sizes have been produced on glass and SiO_2 samples (see Fig.s 3.10 and 5.14), using the protocol given in section 3.2. Also, a chip carrier-mounted circuit was biotinylated and binding of streptavidin-immobilized labels was observed. However, the binding occured all over the chip surface, thus the need to define a mask to expose only the sensor's surface to the biotinylation process. This masking approach is underway and should provide a clearer and easier way to detect the biomolecular interaction.

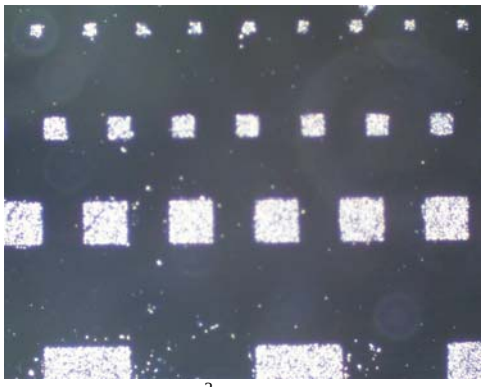
Fig. 5.14: 100×100, 50×50, 25×25 and 10×10μm^2 arrays of 2μm beads on a SiO_2 sample.

An alternative approach also being studied is to deposit a TiW(N_2) layer over the sensor area prior to the addition of the biotinylated cross-linker solution. We have found that the biotin binds to this material without pre-activation, thus providing a selective immobilization procedure. The biotin should bind only to the titanium tungsten nitrate layer (see Fig. 5.15) and the streptavidin beads should then only bind to the biotin, which is restricted to sensor surface.

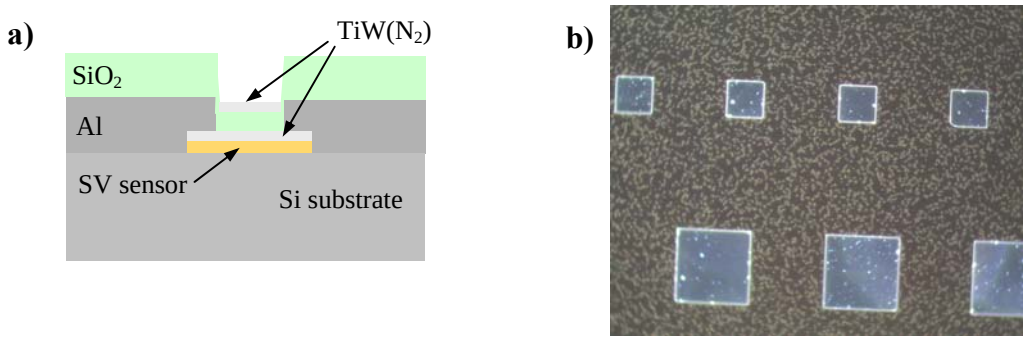

Fig. 5.15: a) Cross-section of the spin-valve sensor site showing the deposited $TiW(N_2)$ layer for selectively binding of biotin (biotin masking). b) 100×100 and 50×50µm^2 inverse arrays of 2µm beads on the titanium tungsten nitrate layer (inverse = only the squares are free of beads due to its glass surface).

6. Conclusions and Future Perspectives

The presented work provides a means to controllably move and detect nanometer or micrometer sized magnetic labels with or without immobilized biomolecules. Furthermore, it successfully demonstrates the detection of a single 2μm superparamagnetic particle with a small number of immobilized biomolecules, namely active HRP enzymes and streptavidin molecules. However, the attached molecules could be DNA and, in principle, be one single DNA molecule.

The present goal is the detection of the binding of streptavidin-functionalized labels to sensor bound biotin, which will demonstrate the use of this system to detect biomolecular recognition. If this is accomplished, as hoped, one can then apply this system to the placement, detection and study of other biomolecules and other biomolecular interactions, in particular single DNA molecules interactions ([29]). Consequently one foresees a wide range of biotechnological applications for this system, including miniaturized high sensitivity biosensors and biochip devices for the screening of proteins and nucleic acids, as also a potential application in *in vitro* or *in vivo* diagnostics, antibody detection and drug research. This is of great importance in the sense that these devices can bring directly or indirectly, improved quality of life, which is translated by the existence of a considerable and growing market for these products ([30]).

This system may also be used also in the study of intermolecular binding strengths, by applying magnetic fields generated either by current lines or by external magnets; or even in frequency modulated interaction studies, by applying time and space varying electric fields.

The fact that a single 2μm bead can be detected, which has ~20 active HRP immobilized enzymes on its surface, opens the possibility of studies of small number of biomolecules. This feature has advantages over traditional biochip systems: as an example, the so called DNA chips and microarrays rely on the detection of large numbers of phosphorescent beads by an expensive optical microscope prepared for these type of measurements. In principle, the biochip idea presented in this work, by using magnetic labels, doesn't need expensive measuring systems, as the sensors can be already on-chip or even in a lower cost system much like a hard disk. This is, in fact, the purpose of the Ph. D the author is about to begin at INESC: build a prototype of a GMR sensor based biochip using magnetic labels. In addition, the studies on small numbers of biomolecules might also reveal some features that cannot be "seen" in bulk samples, which is the conventional way in which biomolecules are studied.

Another idea is to use this system as complementary to others, as for example, with optical and fluorescence systems.

The presented work, has, so far, given rise to the submission of a paper to the Journal of Applied Physics and an oral presentation (by the author) in the 46th Magnetism & Magnetic Materials Annual Conference to happen in next November.

Worthy of mentioning is that, the presented work is part of a project funded last January, POCTI/34459/BIO/2000 – "Detection of Biomolecular Recognition in Nanometer Sized Volumes using Magnetoresistive Sensor Arrays", and more recently

in July was approved as an EC Framework project comprising several European institutions. This aims to apply the presented system to the study and diagnosis of the genetic disease Cystic Fibrosis, QLRT-2001-01982 CF-CHIP – “A novel nanobiotechnology chip platform for detection of genetically heterogeneous genetic diseases: detection of cystic fibrosis as a model”.

A final note: any doubts, questions or comments about this work please feel free to contact the author at the email hatdf@yahoo.com .

"**W**hat I want to talk about is the problem of manipulating and controlling things on a small scale.

As soon as I mention this, people tell me about miniaturization, and how far it has progressed today. They tell me about electric motors that are the size of the nail on your small finger. And there is a device on the market, they tell me, by which you can write the Lord's Prayer on the head of a pin. But that's nothing; that's the most primitive, halting step in the direction I intend to discuss. It is a staggeringly small world that is below. In the year 2000, when they look back at this age, they will wonder why it was not until the year 1960 that anybody began seriously to move in this direction."

(***Richard P. Feynman***, *excerpt of the talk* ***"There's Plenty of Room at the Bottom"*** *gave on December 29th 1959 at the annual meeting of the American Physical Society at the California Institute of Technology*)

Bibliography

[1] - "IBM Travelstar 32GH, 30GT, and 20GN 2.5-inch drives", http://www.storage.ibm.com/hardsoft/diskdrdl/travel/32gh30gt20gndata.htm

[2] - "The era of Magnetoresistive heads", http://www.storage.ibm.com/oem/tech/eraheads.htm

[3] - "MR Heads: The Next Step in Capacity and Performance", http://www.seagate.com /support/kb/disc/mr_heads_tp. html

[4] - "Magneto-Resistive Heads", http://www.seagate.com/support/kb/disc/mrheadfs.html

[5] - P. ten Berge, N.J. Oliveira, T.S. Plaskett, J.L. Leal, H.J. Boeve, G. Albuquerque, J. Ferreira, A.R. Morais, A.T. Sousa, L. Rodrigues, and P.P. Freitas, "Spin-valve MR Heads for Tape and Disk Applications", IEEE Transactions on Magnetics 31, 2603 – 2608, 1995.

[6] - R. Shieh and D. E. Ackley, "Sensing of binding of molecule with receptor at binding site", Motorola patent application PN WO 9745740 (1997).

[7] - D. R. Baselt, G. U. Lee, M. Natesan, S. W Metzger, P. E. Sheehan, and R. J. Colton, "A biosensor based on magnetoresistance technology", Biosensors and Bioelectronics 13, 731-739, 1998.

[8] - Mark Tondra, Marc Porter, and Robert J. Lipert, "Model for detection of immobilized superparamagnetic nanosphere assay labels using giant magnetoresistive sensors", Journal Vacuum Science Technology A, 18 (4), 2000.

[9] - Carl H. Smith, Robert W. Schneider, and Mark Tondra, "Medical Magnetic Biosensors", http://www.sensorsmag.com/articles/1299/14_1299/main.shtml , 2000.

[10] - B. Dieny, V.S. Speriosu, S. Metin, S.S. Parkin, B.A. Gurney, P. Baumgart, and D.R. Wilhoit, "Magnetotransport properties of magnetically soft spin-valve structures", Journal of Applied Physics 69, 4774 – 4779, 1991.

[11] - D.E. Heim, R.E. Fontana, C. Tsang, V.S. Speriosu, B.A. Gurney, and M.L. Williams, "Design and operation of spin-valve sensors", IEEE Transactions on Magnetics 30, 316 – 321, 1994.

[12] - P.P. Freitas, F. Silva, N.J. Oliveira, L.V. Melo, L. Costa, and N. Almeida, "Spin Valve Sensors", Sensors and Actuactors A, 81,2-8, 2000.

[13] - P. Grünberg, R. Schreiber, Y. Pang, M. B. Brodsky, and H. Showers, "Layered magnetic structures: Evidence for antiferromagnetic coupling Fe layers across Cr interlayers", Physical Review Letters 57, 2442-2445, 1986.

[14] - M. N. Baibich, J. M. Broto, A. Fert, F. N. Van Dau, and F. Petroff, "Giant magnetoresistance of (001)Fe/(001)Cr magnetic superlattices ,Physical Review Letters 61, 2472-2475, 1988.

[15] - Gustav J. Strijkers, "Magnetic Nanostructures – an experimental study of structural, magnetic and transport properties", Eidhoven University of Technology, 1999.

[16] - Nuno Oliveira, "Spin-Valve Heads for Tape Applications", Ph. D thesis, February 2000.

[17] - Véronique Gehanno, Paulo P. Freitas, Anabela Veloso, João Ferreira, Bernardo Almeida, J. B. Sousa, A. Kling, J.C Soares, and M.F. da Silva, "Ion Beam Deposition of Mn-Ir Spin Valves", IEEE Transactions on Magnetics 35, 4361 – 4367, 1999.

[18] - J.D. Jackson, "Classical Electrodynamics", 2nd Edition, John Wiley & Sons, 1975.

[19] - "Micromod Partikeltechnologie", http://www.micromod.de/
[20] - "Scientific and Clinical Applications of Magnetic Carriers", Edited by Urs Häfeli, Wolfgang Schütt, Joachim Teller, and Maciej Zborowski, Plenum Press, 1997.
[21] - O. Ryan, M. R. Smyth and C. Ò Fágáin, "Horseradish peroxidase: the analyst's friend", Essays Biochemistry 28, 129-146, 1994.
[22] - "Streptavidin", http://www.genevue.com/A_MModel/Strep_3.html
[23] - Ernst-Ludwig Florin, Vincent T. Moy, and Hermann E. Gaub, "Adhesion Forces Between Individual Ligand-Receptor Pairs", Science 264, 415-417, 1994.
[24] - Vincent T. Moy, Ernst-Ludwig Florin, and Hermann E. Gaub, "Intermolecular Forces and Energies Between Ligand and Receptors", Science 266, 257-259, 1994.
[25] - "Examples of the interactive forces between specific molecules", http://www-ermm.cbcu.cam.ac.uk.00001642h.htm
[26] - "Biotin", http://www.roche.com/vitamins/what/anh/vits/biotin.html
[27] - Hugo Ferreira, "Partículas Nano-Magnéticas", Microtechnologies course report, 21st February 2000.
[28] - Roel Wirix-Speetjens, "Magnetic beads and spin-valves, a step forward in DNA analysis", INESC Report, September 2000.
[29] - M. A. Osbourne, W. Scott Furey, D. Klenerman and S. Balasubramanian, "Single-Molecule Analysis of DNA Immobilized on Microspheres", Analytical Chemistry 72**,** 3678-3681, 2000.
[30] - K. Rubinstein. Biochips: Progress and Prospects 3rd. Ed. Market Analysis Report, D & MD Reports, 2001.

Appendix

A. Immobilization Procedures

For creating arrays, with several sizes, of 2μm microspheres (Micromer®-M) on a sample's surface one proceeds as follows below. The procedure is somehow different according to the sample's surface: differences will be noted when existing. The processes are separated into sample preparation: cleaning, depositing (if needed) and masking; and bead immobilization: activation, cross-linking, binding and washing.

Note: for better understanding of some sample preparation steps please report to section 4.2 Processing.

Bead arrays on a glass sample (as in Fig. 3.9)

Sample preparation

- **STEP 1:** Sample cleaning in Wet Bench
  Substrate:
  Corning Inc. 585879 Glass 7059
  1"×1"×0.16 thickness
  Conditions:
  DI water + Alconox & ultra-sounds
- **STEP 2:** Resist Coating (PR+) in SVG tracks
  Conditions:
  Coater 6/2 speed = 3500 rpm
- **STEP 3:** Mask Exposure in DWL
  Conditions:
  Source file : immobilize [X:15000.000 Y:15000.000]
  Mask: imobilize (L15-inverted)
- **STEP 4:** Mask development in SVG tracks
  Conditions:
  Developer 5/2

Bead immobilization

- **STEP 1:** Surface activation
  Conditions:
  10% aqueous solution of APTS for 30'
  wash in 100mM, pH 7.0 phosphate buffer
- **STEP 2:** Biotin cross-linking to surface
  Conditions:
  0.75mg/ml solution of biotinylated cross-linker for 60'
  wash in 100mM, ph 7.0 phosphate buffer with 10mM NaCl
- **STEP 3:** Binding of Streptavidin to biotin
  Conditions:
  2.5mg/ml solution of streptavidin-functionalized micromer®-M microspheres in 100 mM pH 7.0 buffer for 120'

- **STEP 4:** Resist stripping and washing
  Conditions:
  Rinsing with acetone or Microstrip®2001
  Washing with DI water

Bead arrays on a SiO_2 sample (as in Fig. 5.14)

This procedure only differs from the previous one (for the glass sample) in an extra SiO_2 deposition step in sample preparation.

Sample preparation

- **STEP 1:** Substrate Cleaning in Wet Bench
  Substrate:
  Corning Inc. 585879 Glass 7059
  1"×1"×0.16 thickness
  Conditions:
  DI water + Alconox & ultra-sounds
- **STEP 2:** SiO_2 3000Å Deposition in Alcatel SCM 450
  Conditions:
- **STEP 3:** Resist Coating (PR+) in SVG tracks
  Conditions:
  Coater 6/2 speed = 3500 rpm
- **STEP 4:** Mask Exposure in DWL
  Conditions:
  Source file : immobilize [X:15000.000 Y:15000.000]
  Mask: imobilize (L15-inverted)
- **STEP 5:** Mask development in SVG tracks
  Conditions:
  Developer 5/2

Bead immobilization

- **STEP 1:** Surface activation
  Conditions:
  10% aqueous solution of APTS for 30'
  wash in 100mM, pH 7.0 phosphate buffer
- **STEP 2:** Biotin cross-linking to surface
  Conditions:
  0.75mg/ml solution of biotinylated cross-linker for 60'
  wash in 100mM, ph 7.0 phosphate buffer with 10mM NaCl
- **STEP 3:** Binding of Streptavidin to biotin
  Conditions:
  2.5mg/ml solution of streptavidin-functionalized micromer®-M microspheres in 100 mM pH 7.0 buffer for 120'

- **STEP 4:** Resist stripping and washing
  Conditions:
  Rinsing with acetone or Microstrip®2001
  Washing with DI water

Bead arrays on a TiW(N_2) sample (as in Fig. 5.15b)

This procedure differs from the first one (for the glass sample) in an extra TiW(N_2) deposition step in sample preparation, and also the step of activation in bead immobilization is not needed.

Sample preparation

- **STEP 1:** Substrate Cleaning in Wet Bench
  Substrate:
  Corning Inc. 585879 Glass 7059
  1"×1"×0.16 thickness
  Conditions:
  DI water + Alconox & ultra-sounds
- **STEP 2:** SiO_2 3000Å Deposition in Alcatel SCM 450
  Conditions:
- **STEP 3:** Resist Coating (PR+) in SVG tracks
  Conditions:
  Coater 6/2 speed = 3500 rpm
- **STEP 4:** Mask Exposure in DWL
  Conditions:
  Source file : immobilize [X:15000.000 Y:15000.000]
  Mask: imobilize2 (L15-inverted)
- **STEP 5:** Mask development in SVG tracks
  Conditions:
  Developer 5/2

Bead immobilization

- **STEP 1:** Biotin cross-linking to surface
  Conditions:
  0.75mg/ml solution of biotinylated cross-linker for 60'
  wash in 100mM, ph 7.0 phosphate buffer with 10mM NaCl
- **STEP 2:** Binding of Streptavidin to biotin
  Conditions:
  2.5mg/ml solution of streptavidin-functionalized micromer®-M microspheres in 100 mM pH 7.0 buffer for 120'
- **STEP 3:** Resist stripping and washing
  Conditions:
  Rinsing with acetone or Microstrip®2001
  Washing with DI water

B. Run-sheet (#1)

Spider

Responsible: *Hugo Ferreira*

Sample ID: spider # 1

STEP 1: Substrate Cleaning in Wet Bench

Substrate
3" Si wafer
thickness: 356 - 406 μm
resistivity: 1.0 - 2.0 Ωcm

Date: 05/07/2001
Operator: Hugo Ferreira
Pre-Treatment: No
Conditions:
IPA + DI water + heating @ 130ºC for 30'

Observations:
None

STEP 2: Spin-valve test Deposition in Nordiko 2000

Date: 05/07/2001 to 06/07/2001
Operator: Ricardo Sousa & Hugo Ferreira
Pre-Treatment: No
Conditions:
B.P.: $6{,}7\times10^{-8}$ torr

Ta 73 Å / NiFe 40 Å / CoFe 10 Å / Cu 27 Å / CoFe 29 Å / MnIr 80 Å / Ta 25 Å

Read
Sequence 25 Ric_tests

F18 Ta_buffer	**2'20"**	9,7 **sccm**	4,4 **mT**	**DC2:** 335	**V** 30	**mA**
F20 NiFe_free_layer_I	**1'12"**	9,8 **sccm**	2,5 **mT**	**DC2:** 335	**V** 30	**mA**
F9 CoFe_100W_thin	**12"**	9,8 **sccm**	2,9 **mT**	**RF1:** F101 B178		
F21 Cu_sv_spacer	**36"**	9,8 **sccm**	1,6 **mT**	**DC2:** 306	**V** 30	**mA**
F7 CoFe_200W_I	**35"**	9,9 **sccm**	3,0 **mT**	**RF1:** F101 B178		
F57 MnIr_50mA	**1'08"**	9,7 **sccm**	3,0 **mT**	**DC1:** 312	**V** 50	**mA**
F34 Ta_cap	**50"**	9,8 **sccm**	4,5 **mT**	**DC2:** 317	**V** 30	**mA**

Observations:
Total thickness of the spin-valve material: 284 Å
The function F7 CoFe_200W_I is defined with RF: 100W and not 200W.
Test measurements: spdt1.hug and spdt2.hug

STEP 3: Spin-valve Deposition in Nordiko 2000

Date: 06/07/2001
Operator: Hugo Ferreira
Pre-Treatment: No
Conditions: Same as in step 2

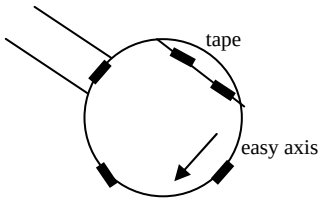

Observations:

STEP 4: TiW(N_2) 150 Å Deposition in Nordiko 7000

Date: 06/07/2001
Operator: Hugo Ferreira
Pre-Treatment: No
Conditions:
Run #7361
Seq. 17 *svpassiv*
Mod3 F19 27" *TiW_Protective_Layer*
50,0 sccm Ar 10,0 sccm N_2 3,0 mT DC: 0,50 kW

Observations:
Needed to adjust manually the process pressure.

STEP 5: Resist Coating (PR+) in SVG tracks

Date: 09/07/2001
Operator: Hugo Ferreira
Pre-Treatment: Vapour – prime (5')
Conditions:
Coater 6/2 speed =3500 rpm

Observations:
Before prime the wafer was washed to clean from stains. After washing the wafer was cleaner.

STEP 6: Mask Exposure in DWL

Date: 09/07/2001
Operator: José Bernardo
Pre-Treatment: No
Conditions:
E: 55 F: 60 Power: 84 mW
Source file: spider [X:8000.000 Y:8000.000]
Mask : spider15 (L15-inverted)
Map: hugo

Observations:
start 17:05 finish 20:38

STEP 7: Mask Development in SVG tracks

Date: 09/07/2001
Operator: José Bernardo
Pre-Treatment: No
Conditions:
Developer 5/2

Observations:
See images.

STEP 8: Spin-valve + TiW(N_2) Etch in Nordiko 3000

Date: 10/07/2001
Operator: Zongzhi & Hugo Ferreira
Pre-Treatment: Clean_assist for 2000"
Conditions:
B.P.: 5×10^{-6} torr
Batch: junction_etch
Etch_gun_stab
Junction_etch
End_etch
Setpoint
Assit Gun: 64 W +500V/-200V 8 sccm Ar
Assist Neutraliser :
Etch time: 1000"
Target #6
Read
Assist Gun: 64 W + 488,5 V/ – 194,3 V + 28,4 mA
– 1,2 mA 7,9 sccm Ar
Assist Neutraliser: 7,6 mA 1,2 V 0,3 sccm Ar
Subst Rotn 40 % Subs Pan 70º
Chamber pressure : $7,6\times10^{-5}$ torr
Target #6 (Ta)

Observations:
First, chamber pressure $8,6\times10^{-5}$ torr. Assist gun plasma out during etch, but it restarted. Etch stoped every 100"- 200".
Later: everything OK! Didn't appear the "Assist gun plasma out – Restrike" message!

STEP 9: Resist Stripping in Wet Bench

Date: 10/07/2001
Operator: Hugo Ferreira
Pre-Treatment: No
Conditions:
Microstrip 2001 @ 80 ºC + ultrasounds

Observations:

STEP 10: Resist Coating (PR+) in SVG tracks

Date: 11/07/2001
Operator: Hugo Ferreira
Pre-Treatment: Vapour – prime (5')

Conditions:
Coater 6/2 speed =3500 rpm

Observations:

STEP 11: Mask Exposure in DWL

Date: 12/07/2001
Operator: José Bernardo
Pre-Treatment: No
Conditions:
E: 55 F: 60 Power: 88 mW
Mask : spider30 (L30 - non-inverted)
Map: hugo

Observations:
Test offset Y = -2,5

STEP 12: Mask Development in SVG tracks

Date: 12/07/2001
Operator: José Bernardo
Pre-Treatment: No
Conditions:
Developer 5/2

Observations:
Some circuits appear to have some stripes, due to exposure. This could damage the die.

STEP 13: Al 5000 Å Deposition in Nordiko 7000

Date: 13/07/2001
Operator: Hugo Ferreira
Pre-Treatment: No
Conditions:
Run #7373
Seq. 33 *svpadnoetch*
Mod2 F9 *contetch* 30" 50,0 sccm 3,0 mT RF1: 70 W RF2: 40 W
Mod4 F1 *alsv* 2'15" 50,0 sccm 3,0 mT DC: 2,00 kW

Observations:
Needed to open manually mod 4 gate valve.
Previous Al deposition measurement gave Al thickness: 4549 ± 207 Å.

STEP 14: Al Liftoff in Wet Bench

Date: 16/07/2001 until 19/07/2001
Operator: Hugo Ferreira
Pre-Treatment: No
Conditions:
Microstrip 2001 @ 80 ºC + ultrasounds

Observations:
Maybe Microstrip 5010 was used: the Al appears brown color (oxidized), nevertheless the big pad contacts work! Also, the spin-valve material seems to have been attacked! Made some sensor viability tests: sp1.hug and sp1b.hug. Think that the main reason that the Al was oxidized is the long time microstrip bath it was subjected to.

STEP 15: SiO_2 3000 Å Deposition in Alcatel SCM 450

Date: 20/07/2001 – 23/07/2001
Operator: Hugo Ferreira
Pre-Treatment: No
Conditions:
Deposition started @ 8:57 finished @ 12:00 (3 hours)
4 rpm / 2,9 mb / 140 W / 20 sccm Ar

Observations:

STEP 16: Resist Coating (PR+) in SVG tracks

Date: 24/07/2001
Operator: Hugo Ferreira
Pre-Treatment: Vapour – prime (5')

Conditions:
Coater 6/2 speed =3500 rpm

Observations:

STEP 17: Mask Exposure in DWL

Date: 24/07/2001
Operator: José Bernardo
Pre-Treatment: No
Conditions:
E: 55 F: 60 Power: 87 mW
Mask : spider10 (L10 - non-inverted)
Map: hugo

Observations: None

STEP 18: Mask Development in SVG tracks

Date: 24/07/2001
Operator: Hugo Ferreira
Pre-Treatment: No
Conditions:
Developer 5/2

Observations:

STEP 19: SiO_2 Ecth in LAM

Date: 25/07/2001
Operator: Virgínia Soares
Pre-Treatment: No
Conditions:
Recipe #6
Setpoint
Ar 200,0 mT / O_2 10,0 mT / CF_4 100,0 mT
He Clamp 16,0
Time 550 s

Read
Ar 201,4 mT / O_2 10,1 mT / CF_4 100,4 mT
CHF_3 0,2 mT / He 0,7 mT / SF_6 0,3 mT / N_2 0,1 mT
He Clamp 16,3 / Bias V – 210 V

Press 140 mT
RF load 102 W
Gap 1,300 cm
Wafer area press 205 mT

Observations:

STEP 20: Resist Stripping in Wet Bench

Date: 25/07/2001
Operator: Hugo Ferreira
Pre-Treatment: No
Conditions:
Microstrip 2001 @ 80 ºC + ultrasounds

Observations:
Process Time : 21 days

Process Completed!

B. Run-sheets (#2)

Spider

Responsible: *Hugo Ferreira*

Sample ID: spider # 2

STEP 1: Substract Cleaning in Wet Bench

Substract
3" Si wafer
thickness: 356 - 406 μm
resistivity: 1.0 - 2.0 Ωcm

Date: 02/08/2001
Operator: Hugo Ferreira
Pre-Treatment: No
Conditions:
IPA + DI water + heating @ 130ºC for 30'

Observations:
None

STEP 2: Spin-valve test Deposition in Nordiko 3000

Date: 02/08/2001 to 03/08/2001
Operator: Hugo Ferreira
Pre-Treatment: First cleaned targets: all_targets
Conditions:
B.P.: $6{,}9\times10^{-8}$ torr
Batch: spin valve
sv11

Ta 20 Å / NiFe 30 Å / CoFe 20 Å / Cu 28 Å / CoFe 25 Å / MnIr 60 Å / Ta 25 Å

Setpoint

Ta4_29mA	**20 Å**	**61"**
NiFe1_29mA	**30 Å**	**73"**
CoFe2_29mA	**20 Å**	**53"**
Cu2_29mA	**28 Å**	**44"**
CoFe1_29mA	**25 Å**	**66"**
MnIr2_29mA	**60 Å**	**167"**
Ta2_29mA	**25 Å**	**76"**
vac_step		**30"**

Read:

Subst Rotn 50% Subst Pan 80º
Chamber pressure: $3{,}8\times10^{-5}$ torr

Observations:

Total thickness of the spin-valve material: 208 Å .

STEP 3: Spin-valve Deposition in Nordiko 3000

Date: 03/08/2001
Operator: Hugo Ferreira
Pre-Treatment: No
Conditions: Same as in step 2

Observations:

STEP 4: TiW(N_2) 150 Å Deposition in Nordiko 7000

Date: 06/08/2001
Operator: Hugo Ferreira
Pre-Treatment: No
Conditions:

Run #7386
Seq. 17 *svpassiv*

Mod3 F19 27" *TiW_Protective_Layer*
50,0 sccm Ar 10,0 sccm N_2 3,0 mT DC: 0,50 kW

Observations:

Needed to adjust manually the process pressure.

STEP 5: Resist Coating (PR+) in SVG tracks

Date: 06/08/2001
Operator: Hugo Ferreira
Pre-Treatment: Vapour – prime (5')
Conditions:

Coater 6/2 speed =3500 rpm

Observations:

STEP 6: Mask Exposure in DWL

Date: 06/08/2001
Operator: José Bernardo
Pre-Treatment: No
Conditions:

E: 55 F: 60 Power: 87,2 - 88 mW
Source file: spider [X:8000.000 Y:8000.000]
Mask : spider15 (L15-inverted)

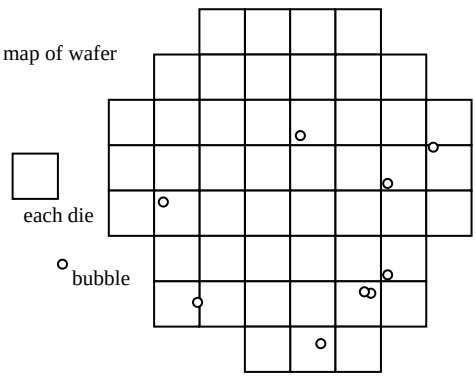

Map: hugo

Observations:

Some dies have bubbles, but seem not be on any relevant structure!

STEP 7: Mask Development in SVG tracks

Date: 06/08/2001
Operator: José Bernardo
Pre-Treatment: No
Conditions:

Developer 5/2

Observations:

See images.

STEP 8: Spin-valve + TiW(N_2) Etch in Nordiko 3000

Date: 07/08/2001
Operator: Hugo Ferreira
Pre-Treatment: None
Conditions:

B.P.: $1{,}2\times10^{-7}$ torr

Batch: junction_etch
Etch_gun_stab
Junction_etch_1
End_etch

Setpoint

Assit Gun: 64 W +500V/-200V 8 sccm Ar
Assist Neutraliser :
Etch time: 1000”
Target #6

Read

Assist Gun: 64 W + 488,8 V/ – 194,3 V + 31,2 mA
– 1,3 mA 8,0 sccm Ar
Assist Neutraliser: 7,6 mA 1,5 V 0,3 sccm Ar
Subst Rotn 40 % Subs Pan 70º
Chamber pressure : $7{,}2\times10^{-5}$ torr
Target #6 (Ta)

Observations:

STEP 9: Resist Stripping in Wet Bench

Date: 08/08/2001
Operator: Hugo Ferreira
Pre-Treatment: No
Conditions:

Microstrip 2001 @ 80 ºC + ultrasounds

Observations:

STEP 10: Resist Coating (PR+) in SVG tracks

Date: 09/08/2001
Operator: Hugo Ferreira
Pre-Treatment: Vapour – prime (5')

Conditions:
Coater 6/2 speed =3500 rpm

Observations:

STEP 11: Mask Exposure in DWL

Date: 09/08/2001
Operator: José Bernardo
Pre-Treatment: No
Conditions:
E: 55 F: 60 Power: 86-87 mW
Mask : spider30 (L30 - non-inverted)
Map: hugo

Observations:
Test offset Y = -2,5

STEP 12: Mask Development in SVG tracks

Date: 09/08/2001
Operator: José Bernardo
Pre-Treatment: No
Conditions:
Developer 5/2

Observations:

STEP 13: Al 5000 Å Deposition in Nordiko 7000

Date: 10/08/2001
Operator: Hugo Ferreira
Pre-Treatment: No
Conditions:
Run #7420
Seq. 33 *svpadnoetch*
Mod2 F9 *contetch* 30" 50,0 sccm 3,0 mT RF1: 70 W RF2: 40 W
Mod4 F1 *alsv* 2'15" 50,0 sccm 3,0 mT DC: 2,00 kW

Observations:
Needed to open manually mod 4 gate valve.
Previous Al deposition measurement gave Al thickness: 4549 ± 207 Å.

STEP 14: Al Liftoff in Wet Bench

Date: 13/08/2001 – 14/08/2001
Operator: Hugo Ferreira
Pre-Treatment: No
Conditions:
Microstrip 2001 @ 80 ºC + ultrasounds

Observations:

STEP 15: SiO_2 3000 Å Deposition in Alcatel SCM 450

Date: 14/08/2001 – 15/08/2001
Operator: Fernando Silva & Hugo Ferreira
Pre-Treatment: No
Conditions:
Deposition started @ 8:00 finished @ 11:00 (3 hours)
4 rpm / 2,9 mb / 140 W / 20 sccm Ar

Observations:

STEP 16: Resist Coating (PR+) in SVG tracks

Date: 15/08/2001
Operator: Hugo Ferreira
Pre-Treatment: Vapour – prime (5')

Conditions:
Coater 6/2 speed =3500 rpm

Observations:

STEP 17: Mask Exposure in DWL

Date: 15/08/2001
Operator: José Bernardo
Pre-Treatment: No
Conditions:
E: 55 F: 60 Power: 90 mW
Mask : spider10 (L10 - non-inverted)
Map: hugo

Observations: None

STEP 18: Mask Development in SVG tracks

Date: 15/08/2001
Operator: José Bernardo

Pre-Treatment: No

Conditions:
Developer 5/2

Observations:

STEP 19: SiO_2 Ecth in LAM

Date: 16/08/2001
Operator: Virgínia Soares
Pre-Treatment: No
Conditions:
Recipe #6
Setpoint
Ar 200,0 mT / O_2 10,0 mT / CF_4 100,0 mT
He Clamp 16,0
Time 450 s

Read
Ar 201,3 mT / O_2 10,1 mT / CF_4 100,3 mT
CHF_3 0,1 mT / He 0,5 mT / SF_6 0,3 mT / N_2 0,0 mT
He Clamp 16,3 / Bias V – 210 V

Press 140 mT
RF load 102 W
Gap 1,300 cm
Wafer area press 207 mT

Observations:

STEP 20: Resist Stripping in Wet Bench

Date: 16/08/2001
Operator: Hugo Ferreira
Pre-Treatment: No
Conditions:
Microstrip 2001 @ 80 ºC + ultrasounds

Observations:
Process Time: 15 days

Process Completed!

C. Process schematics (#1)
spin-valve sensor definition

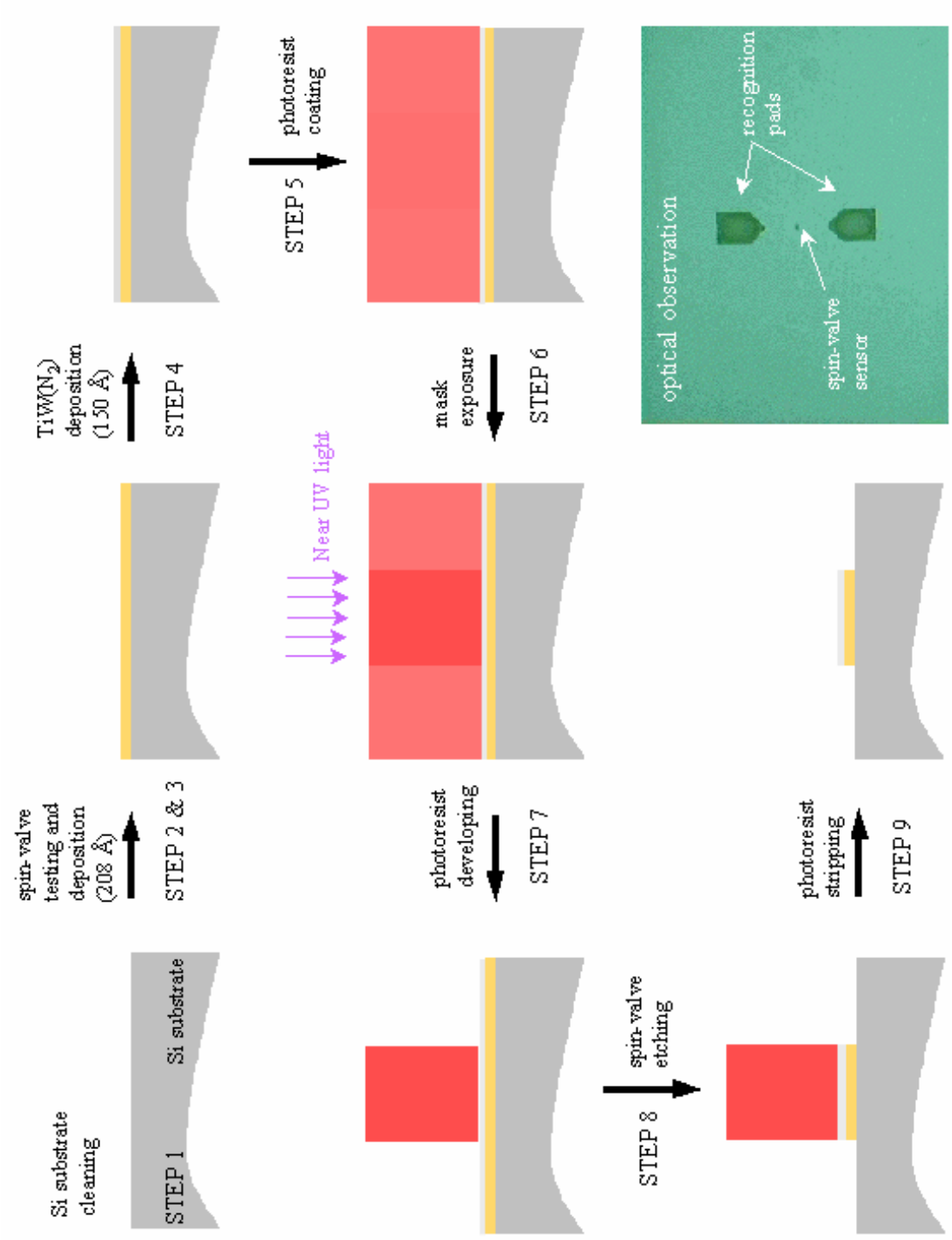

C. Process schematics (#2)
sensor lines and current lines definitions

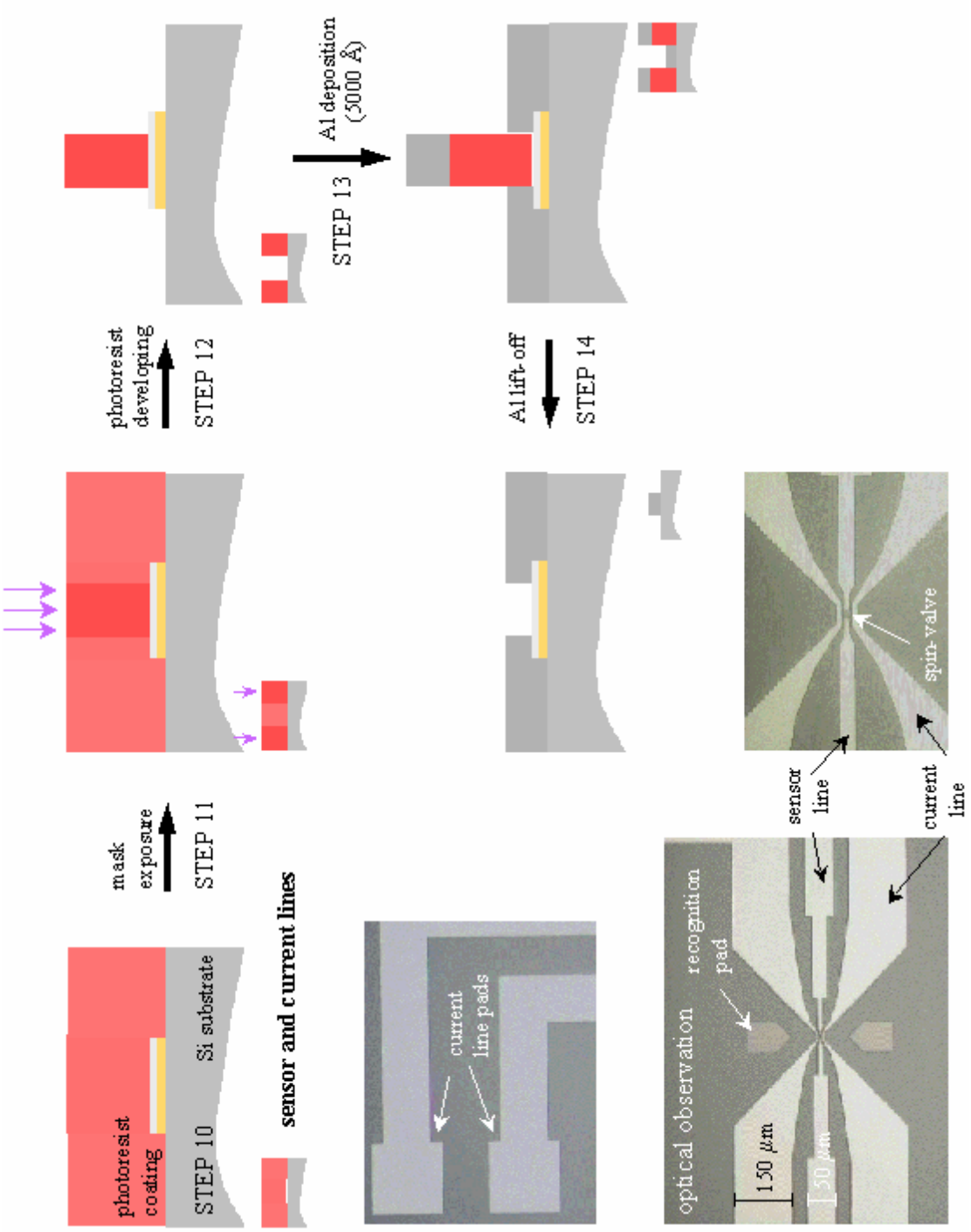

C. Process schematics (#3)
passivation and opening contact vias